Experimental Survey of Spiral Dynamics in the Belousov-Zhabotinsky Reaction

Andrew Belmonte, Qi Ouyang, Jean-Marc Flesselles

J. Phys. II France 7 (1997) 1425–1468 OCTOBER 1997, PAGE 1425

Experimental Survey of Spiral Dynamics in the Belousov-Zhabotinsky Reaction

Andrew L. Belmonte (*), Qi Ouyang (**) and Jean-Marc Flesselles (***)

Institut Non Linéaire de Nice (****), 1361 route des Lucioles, 06560 Valbonne, France

(Received 15 July 1996, revised 7 May 1997, accepted 10 June 1997)

PACS.82.40.Ck – Pattern formation in vortices-diffusion systems
PACS.05.70.Ln – Nonequilibrium thermodynamics, irreversible processes

Abstract. — We present a systematic study of spiral waves in the Belousov-Zhabotinsky reaction in a spatial open reactor, where the concentrations of sulfuric acid, sodium bromate, and malonic acid are varied. Within this parameter space, three kinds of instabilities arise: two of them, which we identify as the retracting wavefront and convective instabilities, lead to the destruction of the spiral pattern, and mark the boundaries of the spiral existence domain in parameter space. Inside this domain, there exists a region where simply rotating spirals undergo the meandering instability. Quantitative measurements of the asymptotic characteristics of simple spirals provide scaling relations between the observables: the pitch varies as the square root of the period. They both diverge with simple exponents at the retracting wavefront instability. This organization, reminiscent of a second order phase transition, allows us to consider the spiral a critical pattern. Comparison with several models and numerical simulations indicates the validity or discrepancies of applying these theoretical approaches to our experimental results.

Résumé. — Nous présentons une étude systématique des ondes spirales dans la réaction de Belousov-Zhabotinsky en réacteur ouvert, en fonctions des concentrations d'acide sulfurique, de bromate de sodium et d'acide malonique. Dans cet espace de paramètres, trois types d'instabilités surviennent : deux d'entre elles, que nous appelons instabilité de rétraction de front et instabilité convective, finissent par détruire les structures spirales, et marquent les limites de leur domaine d'existence. Il existe, dans ce domaine, une région où les spirales en rotation simple bifurquent vers l'instabilité de sinuage. Des mesures quantitatives des caractéristiques asymptotiques des spirales simples fournissent des lois d'échelles entre les observables : le pas varie comme le carré de la période ; tous deux divergent avec des exposants simples à l'instabilité de rétraction. Cette organisation, rappelant celle des transitions de phases du second ordre, nous autorise à considérer la spirale comme une structure critique. La comparaison de nos résultats expérimentaux avec différents modèles et simulations numériques montre accords et désaccords des approches théoriques.

(*) *Present address*: Department of Physics and Astronomy, University of Pittsburgh, Pittsburgh, PA 15260, USA
(**) *Present address:* NEC Research Institute, 4 Independence Way, Princeton, NJ 08540, USA
(***) *Present address:* Laboratoire Physique et Mécanique des Milieux Hétérogènes, École Supérieure de Physique et Chimie Industrielles, 10 rue Vauquelin, 75231 Paris Cedex 05, France. Author for correspondence (e-mail: flessel@pmmh.espci.fr)
(****) UMR 6618 CNRS-UNSA

Table of Contents

1. Introduction

In his book *On Growth and Form*, D'Arcy Thompson speculated that a quantitative description of natural patterns and forms, or what he called "a dynamical morphology', would originate from a consideration of geometrical constraints and the physical laws of nature [1]. The realization of this goal is far from complete, but much information on the dynamics of patterns has been gained in recent years [2–4]. These efforts intersect the formal theoretical study of nonequilibrium systems, due largely to the work of the Brussels school [5,6]. A major achievement in these areas was made by Turing in 1952 [7]. He mathematically showed that a spatial pattern can spontaneously arise from homogeneous initial conditions in a reaction-diffusion system, and proposed this as a possible explanation for morphogenesis. His work initiated numerous investigations of reaction-diffusion systems.

Such reaction-diffusion systems are ubiquitous in nature: in addition to morphogenesis, they may be responsible for many other forms, structures and patterns that arise in the living world [8]. They consist of a spatially extended system, where local concentration changes are due to either local reactions or to diffusion due to local gradients. This definition excludes mixing and other bulk motion. A great amount of work has been devoted to the analysis of

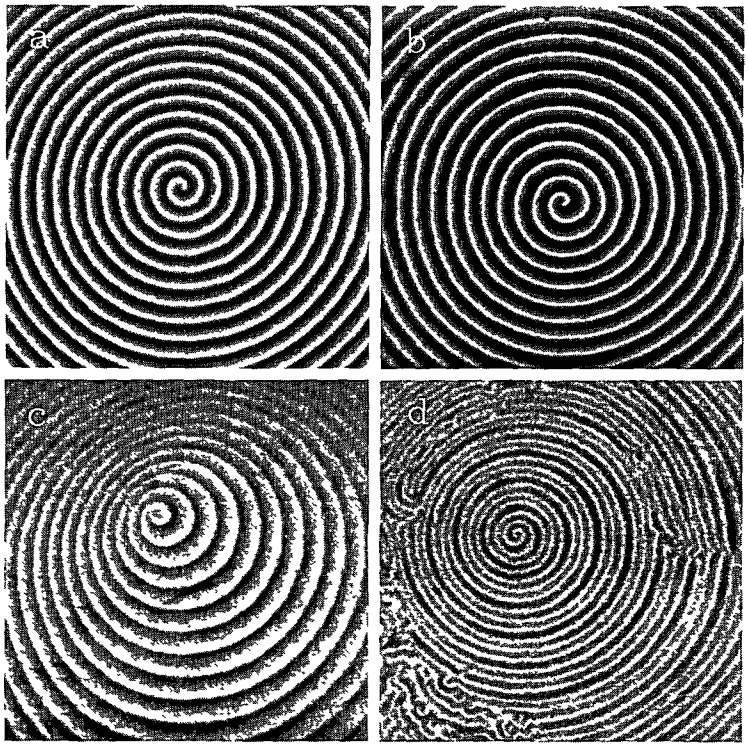

Fig. 1. — An experimental zoology of spiral shapes from the ($[H_2SO_4]$, $[NaBrO_3]$, [MA]) parameter space: (a) simple: (0.20 M, 0.40 M, 0.40 M); (b) small meandering: (0.50 M, 0.15 M, 0.80 M); (c) large meandering: (1.0 M, 0.10 M, 0.04 M); (d) Eckhaus instability: (0.65 M, 0.40 M, 0.40 M). See Section 2.2 and Table I for experimental details.

the wide variety of patterns which develop in reaction-diffusion systems, but there is not yet a general theory giving the common characteristics of the stable, hence observable, solutions. These questions are fundamentally related to a problem pointed out by Feynman in his *Lectures on Physics*: we have no general *qualitative* understanding of the solutions of partial differential equations [9]. This represents one of the most profound shortcomings of modern physics and mathematics.

A rotating spiral wave provides a simple case of a reaction-diffusion pattern that is experimentally tractable and nevertheless retains enough of the richness of the general problem. In the experiments we report here, we observe a variety of different spirals, several of which are shown in Figure 1. Spiral waves are mainly, though not exclusively, observed in a class of reaction-diffusion systems called excitable media [10]; if properly stimulated, such media can sustain propagating fronts. Archetypal excitable media are nerves and cardiac muscles [11–13], but these require delicate experimental handling. Under appropriate conditions, the Belousov-Zhabotinsky reaction provides an adequate excitable system, suitable for controlled laboratory experiments.

Since the original publication by Zaikin and Zhabotinsky on the wave sustaining property of what is now known as the Belousov-Zhabotinsky (BZ) reaction [14], and the seminal article on spirals by Winfree [15], a large amount of work has been devoted to these remarkable patterns;

the reader can find a recent overview in [16]. Many qualitative properties of either free of forced spirals have been observed and analyzed, experimentally or theoretically. Their most basic and striking properties were already summarized in the abstract of Winfree's article: "The Zaikin-Zhabotinsky reagent propagates waves of chemical activity. Reaction kinetics remain to be fully resolved, but certain features of wave behavior are determined by purely geometric considerations. If a wave is broken, then spiral waves, resembling involutes of the circle, appear, persist, and eventually exclude all concentric ring waves" [15]. Although these spiral waves are intrinsically out-of-equilibrium patterns, most studies have been conducted in closed reactors, where the system is (slowly) relaxing to equilibrium. Few experiments have been run in open reactors where the "distance to equilibrium" can be imposed and controlled [17–19]. Hence quantitative results are scarce. In particular, there is essentially no way to quantitatively compare spirals made in reagents with different concentrations.

In this article, after a rapid presentation of the BZ reaction, and of our experimental method, we report our results on the behavior and stability of a single spiral. They are threefold: first, the phase diagram structure in the parameter space that we have explored; second, the description of the observed instabilities, which either limit the existence domain of the spiral, or modify its dynamical behavior; third, a set a quantitative laws, which link these results with the actual concentrations of the chemical species, and show that the spiral can be considered a "critical pattern". At the end of the article, we analyze our results in view of existing theories, and compare them to other available experimental studies.

2. Description of Experiment

2.1. Belousov-Zhabotinsky Reaction Overview. — Because of the remarkable property of exhibiting oscillations during a long transient approach to equilibrium, the BZ reaction has served as a prototype of nonlinear dynamical systems in chemistry, and has been thoroughly studied both experimentally and theoretically. When it was first discovered in the 1950's by Belousov [20], it was generally thought that such behavior was forbidden by thermodynamics; the scientific community refused to accept it. Nevertheless, the recipe circulated in the Soviet Union, and was proposed as a Ph. D. subject to Zhabotinsky in 1961 [21]. Few outside of the USSR knew of the existence of such a reaction until its publication in 1970 [14]. It has been widely studied since it is simple to perform, visually striking, and an abundant source of phenomena. In a well-stirred beaker, the oscillations can be easily observed by the naked eye, since the solution changes color between blue and red. When confined to a thin layer, the system can produce different dynamical patterns, such as targets or spiral waves.

From a chemical point of view, the BZ reaction is the oxidation by bromate of an appropriate organic species catalyzed by a metal-ion/organic-compound complex in an acidic solution [22]. Possible organic acids include carbonic acid, the dicarboxylic acids, the ketons, the diketons, citric acid, and malonic acid, and possible metal ions include Ce^{3+}, Mn^{2+}, Fe^{2+}, Ru^{2+}, Cr^{2+} or Co^{2+} [23]. Though the initial discovery was made using citric acid with a cerium catalyst, the most commonly used organic species are malonic and bromomalonic acid, and the most common catalysts are Mn^{2+}, $Fe(phen)_3^{2+}$ (ferroin) and $Ru(bpy)_3^{2+}$ (ruthenium). Soon after its publication, chemical mechanisms were proposed that can be translated into kinetic equations [24, and references therein]. Nevertheless, a full elementary chemical description of the underlying processes has not yet been agreed upon.

Many studies have been devoted to the diverse behavior exhibited by this reaction: transient oscillations in batch (closed) reactors [24], or sustained oscillation and chaos in continuously fed stirred tank (open) reactors (CSTRs) [25]. Because they are well mixed, these systems are homogeneous, and can be considered zero dimensional. Qualitative new phenomena appear

when spatial degrees of freedom are introduced. This is achieved by constraining the solution in the desired geometry with no stirring, to allow for spatial gradients. When appropriate experimental precautions are taken, diffusion is the only other mechanism added to the reaction [26, 27].

Here we focus on the two-dimensional (2-D) case. The reagent can be prepared such that it is no longer self-oscillatory, but remains in the reduced catalyst state, requiring a local stimulation (local potential pulse or acid excess) in order to trigger an oxidation wave. This property, called *excitability*, is a basic concept in biology. In particular, it has been used to describe nerve impulse propagation [28] and cardiac waves on the surface of the heart [29]. The BZ reaction is well known as a convenient laboratory medium for the study of excitable systems [12]. In our study, we have not systematically analyzed nor distinguished the experimental conditions in which the medium is excitable or oscillatory, since it does not seem to affect the characteristics of the spirals.

For most concentrations of the BZ reaction, spirals do not appear spontaneously, but have to be created. A simple way to do this is to break an oxidizing front, either mechanically with a gentle local disturbance, or chemically by locally inhibiting the reaction. Once a front is broken, the two free ends start to curl up and eventually form two stable spirals of opposite chirality, spinning at the same rate.

2.2. EXPERIMENTAL SETUP. — Our experiment was conducted in a spatial open reactor which was first described in [30], and is similar to the one used for the study of Turing patterns [31]. The reactor allows for the study of true asymptotic states, since the chemical reagents are continuously refreshed. It is the 4th generation of the spatial open reactors developed in Bordeaux [32,33] and Texas [17,34]. Our reactor was built at the University of Texas at Austin.

The heart of our reactor is a thin porous glass disk (Vycor glass, Corning), 0.4 mm thick and 25.4 mm in diameter, which serves as the matrix for the chemical reaction. The porous glass disk is used to prevent hydrodynamic motion in the reaction medium; it has 25% void space and 100 Å average pore size. It is translucent, and inert to the BZ reaction. The diffusive motion which occurs within it has a diffusion constant $D < D_{H_2O}$. For the BZ components in an aqueous medium, a value of $D = 2.0 \times 10^{-5}$ cm^2/s has been measured [35]. For Vycor, an estimate of the effective diffusion constant relevant to waves in the BZ reaction can be made by comparing the pitch of two spirals in the same chemical solution, one in Vycor and the other in aqueous medium restricted to have the same thickness [36]. One finds $D \simeq 4.2 \times 10^{-6}$ cm^2/s, in fair agreement with other measurements [37]. Another diffusion constant, namely the transverse diffusion constant across the porous glass, has been measured with a gradient of ions: $D_\perp \simeq 7 \times 10^{-7}$ cm^2/s [38]. However, the in-plane coefficient is more relevant to our spiral patterns. This subject is in need of more precise measurement.

The porous glass provides a reaction medium homogeneous over at least a distance of two or three spiral wavelengths (~1 mm). A slight inhomogeneity on larger length scales (~10 mm) is observed in some porous glass. However, in our experiment, its presence did not influence the dynamical behavior of the spiral tip, and had little effect on the chemical waves. Different Vycor porous glass disks differ by a few percent in their thickness and density, so that changing the disk may induce a shift in the parameter space. In order to avoid this, the same piece of porous glass was used throughout the entire experiment.

The reactor itself is comprised of two Plexiglas halves, each a CSTR 7.5 ml in volume (Fig. 2). Each CSTR is agitated by two magnetic stir bars at the bottom, and the chemicals are delivered by a peristaltic pump (Ismatec IPC-8) at a rate of 67 ± 1 ml/h (residence time of about 15 min). The porous glass disk is attached to a Plexiglas holder with silicone glue, and is held between the two CSTRs so that each side is in contact with a bulk medium where the

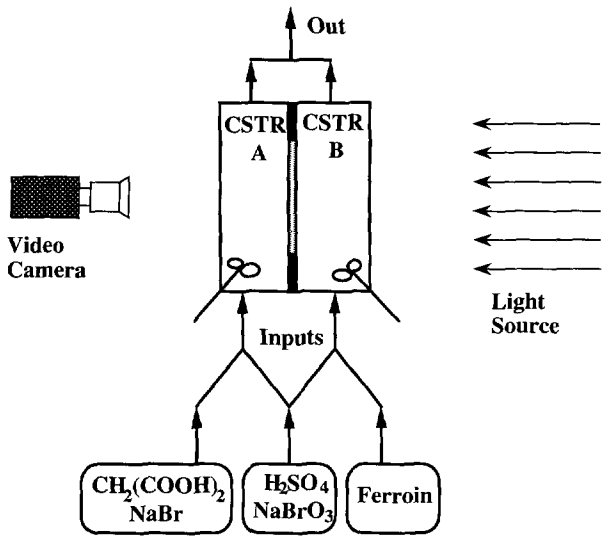

Fig. 2. — A diagram of our experimental setup with the arrangement of the chemical species.

chemical concentrations are kept constant and homogeneous. The whole reactor is surrounded by a copper thermal jacket, with which the temperature was regulated to within 0.1 °C.

We use malonic acid as the organic species, and ferroin ($Fe(phen)_3^{2+}$). a complex of iron and (1.10) phenanthroline as the catalyst. The components of the reaction are distributed in such a way (see Fig. 2) that multi-gradients in chemical concentrations exist normal to the plane of porous glass disk: malonic acid ($CH_2(COOH)_2$, abbreviated MA) is supplied only to CSTR A, and ferroin only to CSTR B. This means that the actual values of these concentrations within the porous glass are unknown, and that the location where the pattern forming reaction takes place may vary. The other chemical species, sodium bromate ($NaBrO_3$), and sulfuric acid (H_2SO_4) are fed in equal amount to both CSTRs. A certain amount of sodium bromide and Sodium Dodecyl Sulfate (SDS) ([SDS] = 0.1 mM) is also fed into CSTR A to keep the bulk from oscillating and to prevent large bubbles from forming [39, 40]. Without the catalyst, the chemicals in CSTR A are not reactive. In CSTR B ferroin reacts immediately (within a second) with bromate to produce ferriin ($Fe(phen)_3^{3+}$) in the presence of sulfuric acid. In order to maintain the chemical gradients across the reaction medium, the flow rate of the CSTRs must be much larger that the diffusive flux across the porous glass disk. The diffusive flux was estimated to be 2 ml/h, much smaller than the pump flow rate. We have not studied the influence of the flow rate in detail.

The arrangement shown in Figure 2 imposes practical limits on the maximum concentrations which can be used for a given flow rate. For [MA] > 0.6 M, we observe that the bulk of CSTR B begins to oscillate below a certain value of $[H_2SO_4]$. This means that enough malonic acid is diffusing into CSTR B to induce the full BZ reaction in the bulk. However, the observations on spiral dynamics made in the presence of these oscillations did not show any differences with lower [MA], where the oscillations are suppressed. Thus the spiral is insensitive to these oscillations.

The reactants from each CSTR diffuse into the porous glass disk where the pattern-forming reaction takes place. For a typical set of concentrations, traveling waves spontaneously appear. They are emitted either by sources at the boundary or by spirals. Early experiments showed

Table I. — *Parameters for the BZ reaction in our experiments. The superscripts on the concentrations indicate the CSTR into which each species is fed.*

$[H_2SO_4]^{AB}$	$[NaBrO_3]^{AB}$	$[CH_2(COOH)_2]^{A}$	$[\text{ferroin}]^{B}$	$[NaBr]^{A}$	temperature	flow rate
0.03–1.0 M	0.05–0.6 M	0.04–1.0 M	1.0 mM	30.0 mM	23 ± 0.1 °C	67 ml/h

that the sources at the boundary have a higher frequency than the spirals, and thus gradually destroy them [17]. To eliminate this problem, we make the area of reaction medium in contact with CSTR A (the malonic acid side) slightly larger than that in contact with CSTR B (the ferroin side), by using an asymmetric Plexiglas holder. This results in a boundary condition along the perimeter of the porous glass disk for which the malonic acid concentration is higher, and ferroin lower, than elsewhere. The result is that the sources at the boundary have a lower frequency than the spirals in the reaction medium. Thus the spiral waves also act to suppress these pace-makers, and dominate the system.

We have found that the spirals in our system are sensitive to red light, by using either a diode (3 mW, $\lambda = 670$ nm) or helium-neon laser (1 mW, $\lambda = 633$ nm). It has been known for some time that the ferroin-catalyzed BZ reaction can be affected by visible light [41, 42], though it has not been used in pattern-forming experiments until recently [30, 43]. Studies using light in the ruthenium-catalyzed system have been more common [44–46]. The reduction of ferriin to ferroin is known to be accelerated by light in the range of 580–700 nm, but the detailed chemical processes are still not understood [42]. This effect allows us to manipulate the spirals in the system by focusing the light beam on the center of the spiral. Initially if there are many spirals, we bring one spiral to the center and drive the rest to the boundary. If there is no spiral in the beginning, we create a pair of counter-rotating spirals by using light to break the wavefront. Then the same technique is employed to remove one of them.

For an experimental survey of the BZ reaction in an open reactor, a large number of external parameters are available: temperature, the chemical flow rate through the reactor, and five chemical concentrations. We restrict ourselves to three variables: the input concentrations of sulfuric acid, sodium bromate, and malonic acid, which we vary within a range of about 0.03 to 1 M. The other parameters are held fixed at: [NaBr] = 30 mM, [ferroin] = 1.0 mM, and temperature 23 ± 0.1 °C, with a flow rate of 67 ml/h. The experimental conditions are summarized in Table I.

We choose $[H_2SO_4]$ and $[NaBrO_3]$ as control parameters since it is known that the speed of waves in the medium depends primarily on these two species, and is by comparison independent of ferroin and malonic acid [47,48]. Malonic acid plays a unique role since it is consumed during the reaction cycle (see Sect. 2.1). This is a crucial point for closed systems, which eventually run out of malonic acid. Thus, although there is no such limitation in an open system, the concentration of MA is potentially interesting. Indeed, qualitative changes actually do occur as [MA] is varied.

Once a single spiral has been prepared, it is studied by changing stepwise (increasing or decreasing) one chemical concentration while fixing the others. Enough time is allowed between changes so that the system can relax to its new asymptotic state. The typical waiting time is 1 to 2 hours (4 to 8 residence times).

2.3. MEASUREMENT TECHNIQUES. — Our raw data are images. They originate from a charge coupled device camera (Sony XC-77CE) and are either grabbed directly onto a computer or are stored onto a Hi8 video recorder (Sony EVO-9650P) for later processing. The frame grabber (Image VGA+, Mu Technologies) digitizes the input signal into a 256 gray level, 512×726 pixel

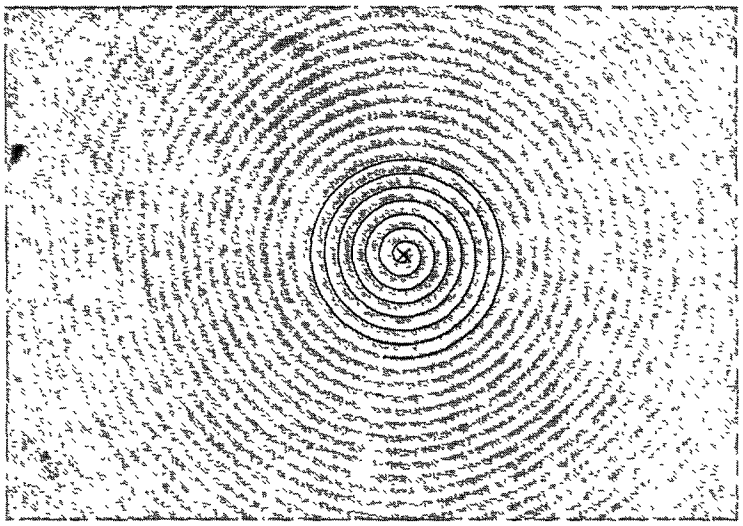

Fig. 3. — A typical single spiral wave in our experiment, with the best fit Archimedean spiral superimposed. Note the edges of the reactor (diameter 2.0 cm).

image. Special care was taken to have true square pixels, and thus to avoid spatial distortion. The field of view was chosen to cover the largest useful part of the cell: a typical image represents about 19 mm × 13.5 mm, with a resolution of 26.4 μm/pixel. Our images are usually well contrasted, with clear features: the spiral appears as a light front over a dark background, as shown in Figure 3.

Müller *et al.* have shown that the shape of a simply rotating spiral in the BZ reaction is experimentally indistinguishable from an Archimedean spiral or from the involute of a circle [49]. The algorithm they used to extract the geometric and kinematic characteristics of a spiral has two parts. First, they find either the highest intensity pixels, which are close to the middle of the wavefront, or the lowest intensity ones, which are between two fronts. In the second part, the Cartesian coordinates of the selected pixels are transformed into polar coordinates, and a nonlinear fitting routine is used to find the parameters of the spiral (Archimedean or involute) that provide the best agreement with the experimental points.

Since our spirals often have up to 20 turns, whereas Müller *et al.* were working with at most 2 or 3 turns, their algorithm would have been too time consuming. In addition, the small deviations from the Archimedean shape that are important in the neighborhood of the spiral center become negligible a few turns away. Our algorithm relies on the assumption that the shape of the spiral is Archimedean, *i.e.* a curve best described in polar coordinates, where the radius r varies linearly with the polar angle θ:

$$r_{\mathrm{A}}(\theta) = \frac{p}{2\pi}(\theta - \theta_0), \quad \text{with } \theta \geq \theta_0, \qquad (1)$$

where p is the pitch of the spiral, and θ_0 the angle of the spiral with respect to a reference axis. The two possible chiralities (clockwise or counterclockwise) are described by choosing the direction in which the angle is increased.

Our computer program extracts the location of the edge of the spiral front from its maximum contrast side, and then finds the best-fit Archimedean spiral. The user indicates the chirality and provides an estimated center and outer radius by clicking on the image. Starting from the

outer radius and moving inwards, the program finds the radial position of the front at equal angle steps from the estimated center, until it arrives at the center. The collection of points $r(\theta)$ gives a straight line if the estimated center is the true one; otherwise a sinusoidal component is superimposed. The average straight line is subtracted and the projection of the modulation onto the sine and cosine functions are calculated. They are proportional to the offset vector $\delta\mathbf{r}$ between the true center and the estimated one. The center of the coordinate system is then corrected, and the entire procedure is iterated until the corrections to the center become small enough (arbitrarily chosen to be a hundredth of a pixel). For usual cases, convergence is obtained in 3 or 4 iterations. In Figure 3, the best fit Archimedean spiral is superimposed on the experimental image.

The period can be obtained by following θ_0 as a function of time, but is usually measured by stopwatch over many rotation periods (usually between 5 and 10).

3. Results

3.1. PHASE SPACE STRUCTURE. — We start with a simple observation. For a given set of the external parameters, a spiral either *exists* or it does *not* [1]. If it exists, it is either *regular* (this corresponds to a nearly Archimedean spiral, undergoing simple, rigid-body rotation), *distorted* (the pitch looks uneven, and the spiral is meandering), or *unstable* (to three different instabilities described below). This defines different regions within the three dimensional parameter space. Note that none of the boundaries are "fuzzy": all of the transitions are direct.

Figure 4 contains the framework which encompasses our experimental study: four phase diagrams corresponding to four different planes in the 3-D parameter space. About 200 different points are included in this survey, each labeled according to the observed pattern: simply rotating spiral "S", meandering spiral "M", or convectively unstable spiral "C"; the other possibilities are a disordered, turbulent state "T", or no pattern at all. There is a sort of balloon in parameter space within which spirals can exist; its boundaries are defined by the instabilities of the spiral. This divides parameter space into three domains: the balloon interior, in which either simple or meandering spirals occur, and the two homogeneous states, either chemically oxidized or reduced. In the lower left corner of Figures 4a-c, where either the concentration of H_2SO_4 or $NaBrO_3$ is low, the medium is homogeneously red, corresponding to a completely reduced catalyst. At the other limit, when these concentrations are high enough, a homogeneously blue medium is observed, corresponding to a completely oxidized catalyst. The low concentration boundary (square symbols) represents a simple transition from spirals to a reduced (red) state, occurring, within our experimental precision, at a single line which coincides with what we identify as the *retracting wavefront instability* (see Sect. 3.2.1). The boundary between the spiral region and the oxidized state (circle symbols) is more complicated, since there the spiral undergoes a convective instability leading to defect-mediated turbulence.

The first three diagrams, each taken at different fixed [MA], have a similar structure: the spiral existence boundaries hardly vary with [MA]. But [MA] strongly affects the transition between simple rotation and meandering. At [MA] = 0.04 M (Fig. 4a), only meandering spirals are observed, whereas at [MA] = 0.4 M (Fig. 4b), only simply rotating spirals are observed; at [MA] = 1.0 M (Fig. 4c), both simple and meandering spirals are observed. The fourth phase plane (Fig. 4d) was taken perpendicular to the previous three at fixed [$NaBrO_3$] = 0.15 M, chosen so as to intersect the meandering transition at [MA] = 1.0 M (Fig. 4c). One clearly

[1] By this we mean, is it possible to maintain a spiral pattern for the given conditions? The spiral is usually created at other values of the parameters, which are then slowly changed to the ones under study.

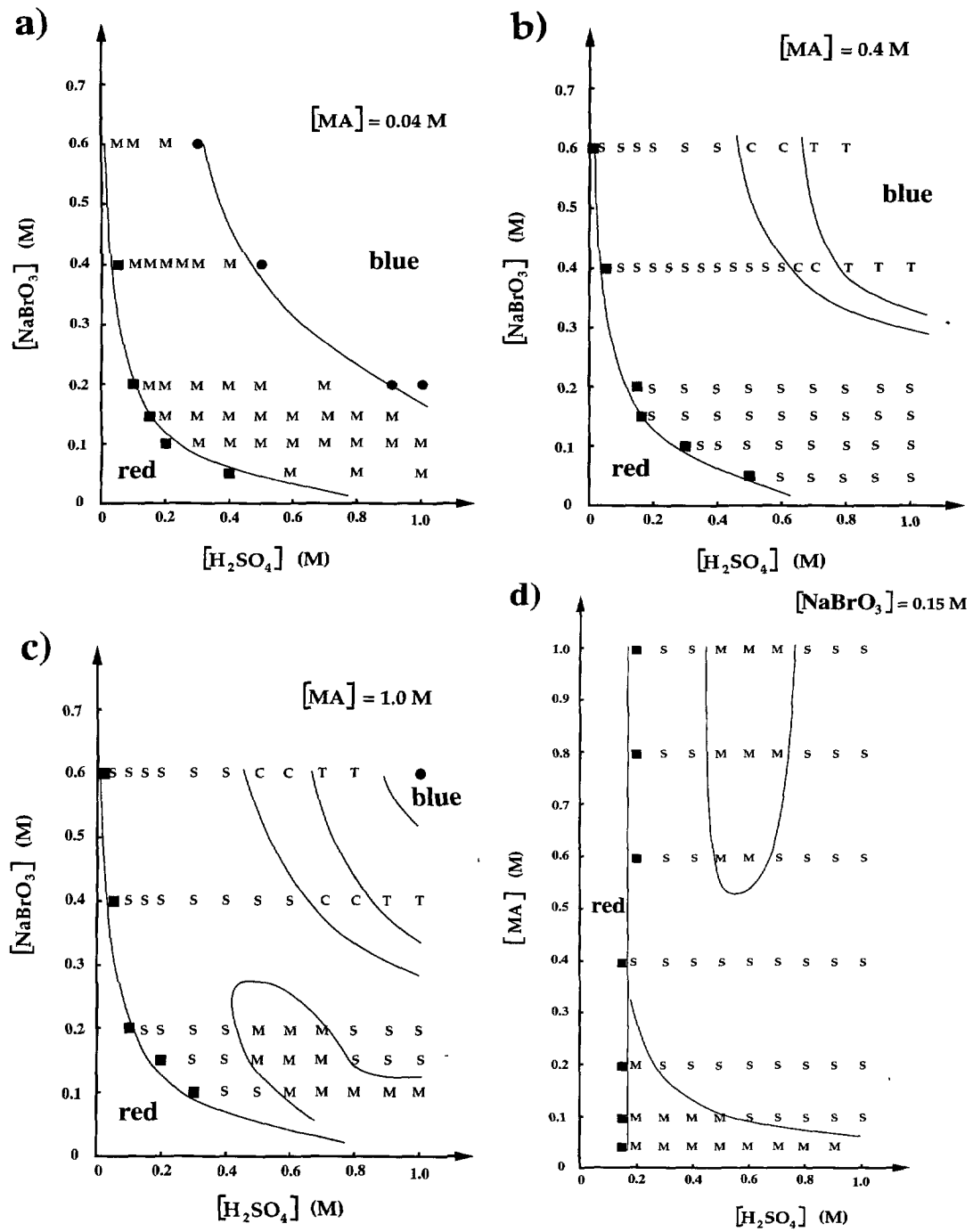

Fig. 4. — The four phase diagrams studied in our experiments. Three planes of ($[H_2SO_4]$, $[NaBrO_3]$) at: (a) [MA] = 0.04 M; (b) [MA] = 0.4 M; (c) [MA] = 1.0 M; (d) the plane ($[H_2SO_4]$, [MA]), at $[NaBrO_3]$ = 0.15 M. The symbols represent: S, simple spiral: M, meandering spiral; C, convectively unstable spiral: T, turbulent state. The black squares represent the retracting wavefront instability, and the black circles correspond to the observation of a homogeneously blue medium. The lines are meant to guide the eyes.

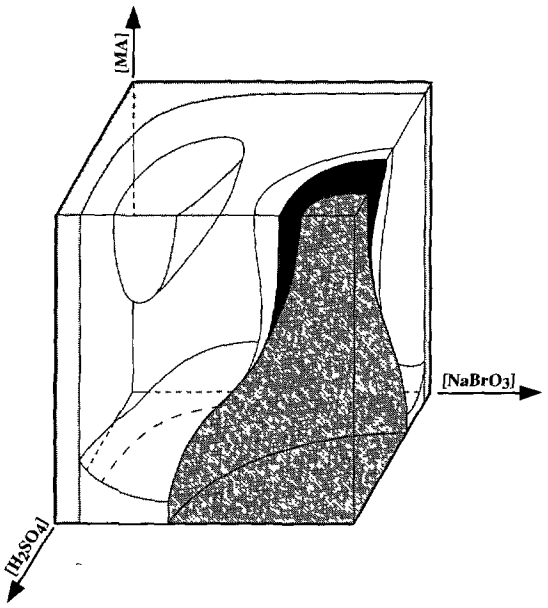

Fig. 5. — Three dimensional representation of the explored phase diagram extrapolated from the data in Figure 4. The three concentrations vary between about 0.04 and 1 M. The backmost (medium dark gray) state is the homogeneous (red) reduced state. The frontmost (dark gray) state is the homogeneous (blue) oxidized state. Next to it are the turbulent (black) and convective instability (light gray) state. The medium light gray regions correspond to the meandering spirals. The rest (transparent white) are the simple spirals. For more details, see text and Figure 4.

sees a "re-entrance" of meandering in the ($[H_2SO_4]$, [MA]) parameter plane: starting from [MA] = 1.0 M, the meandering instability disappears as [MA] is decreased, then reappears again at low [MA]. Thus with all other concentrations fixed, one sees two transitions from simple to meandering by varying [MA].

The overall qualitative structure of this three-dimensional phase space is represented in Figure 5. Note that it is an extrapolation and a qualitative summary of the actual data represented in the four phase diagrams. One clearly sees the striking geometry of the two meandering regions (medium light grey in the figure); are they connected? Also, we have not seen any instabilities along the [MA] axis which limit the existence balloon, though they surely must exist, at least for low enough [MA] (below 0.04 M), which we have not investigated.

3.2. Spiral Instabilities. — We have observed three different spiral instabilities in our experiment. These correspond to cases in which either the fronts break apart and the ends do not curl up, the spiral structure itself loses its stability, or a second frequency appears in the motion of the spiral tip. The first two cases account for the boundaries of the spiral stability balloon in the (H_2SO_4, $NaBrO_3$) plane. The third case corresponds to meandering, a modulating instability which does not destroy the spiral. In a slightly different experimental situation, we have observed another case, in which the center of the spiral is destroyed, but we will not discuss it here [50].

3.2.1. Transition to the Chemically Reduced State: Retracting Wavefront Instability. — The lower boundary in our four phase planes represents some minimum condition for the existence

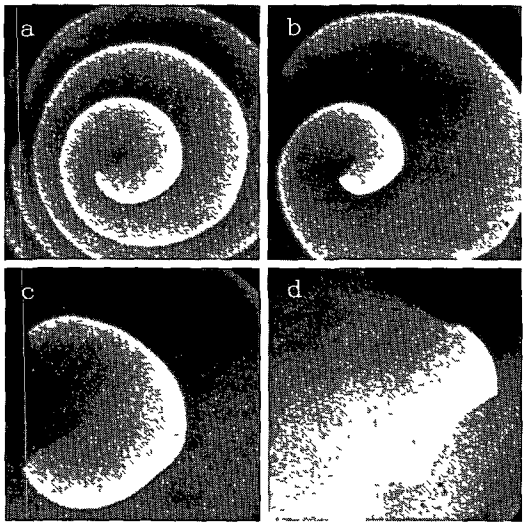

Fig. 6. — Four progressive images of the retracting wavefront instability, as the spiral reaches the edge of the stability boundary: (a) t = 0 min; (b) t = 6 min; (c) t = 10 min; (d) t = 18 min.

of spirals. In this region the medium is excitable. At the critical line, the spiral disappears, and beyond it, the medium is in the reduced state. The experimental points defining this boundary are the critical concentrations ($[H_2SO_4]_C$, $[NaBrO_3]_C$). The simplest fit of $1/[NaBrO_3]_C$ *vs.* $[H_2SO_4]_C$ is a straight line going through zero, as shown in Figure 7 for the three phase diagrams at fixed [MA]. This implies the relation:

$$[H_2SO_4]_C \times [NaBrO_3]_C \equiv \chi_c = 0.022 \pm 0.003\ M^2. \quad (2)$$

Thus the critical line is a hyperbola, which provides a quantitative minimum condition for the existence of spirals: $[H_2SO_4] \times [NaBrO_3] > \chi_c$. It also identifies what we will later show to be the control parameter for the spiral.

The instability associated with this critical line is illustrated in Figure 6, for which we have observed three qualitative characteristics. First, the spiral rotates more slowly as this line is approached, and indeed its frequency vanishes at the line (see Sect. 3.3.1). Secondly, large sections of the wavefronts simply disappear, resulting in a break. This break takes place in preferred regions of the cell, probably related to inhomogeneities of the porous glass. Thirdly, the free ends of these broken fronts usually do not curl up and form new spirals, but instead retract, a clear indication of a condition for which spirals cannot exist.

As seen in Figure 7, there is no significant difference in the critical line at each [MA]. This is particularly interesting for [MA] = 0.04 M, implying that the critical line defined by equation (2) applies equally to meandering and simply rotating spirals. However, at high [MA] (> 0.6 M), the bulk is oscillatory at the critical line. This affects the wavefront which tends to vanish through some kind of wave amplitude collapse. Also, the free ends still tend to curl up, though slowly.

Though we have not observed a continuously retracting wavefront without front breaking, we interpret this boundary as the location of the "retracting wavefront" transition that is observed elsewhere [51–55]. We believe that the other phenomena either come from the setup (global bulk oscillations) or from the narrowness of the stability region for wave propagation.

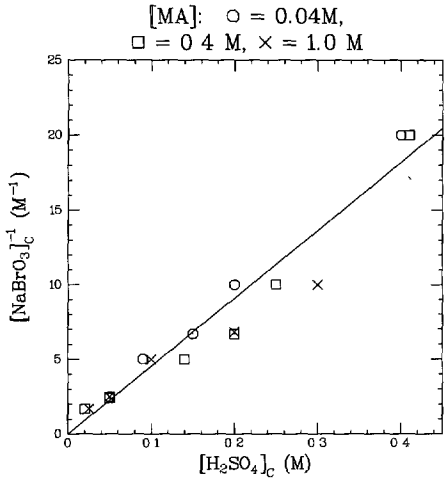

Fig. 7. — A plot of the critical values $1/[NaBrO_3]_C$ *vs.* $[H_2SO_4]_C$, for various [MA]. The line shows the best fit hyperbola, representing the condition $[NaBrO_3]_C \times [H_2SO_4]_C = \chi_c$, as defined in the text.

Our experimental procedure does not allow us to observe this stability region for retracting wavefronts, nor to distinguish this spiral stability boundary from the boundary of wave stability [56, 57]. However we have not searched for these distinctions in detail.

3.2.2. Transition to the Chemically Oxydized State: Eckhaus Instability. — This instability was first reported in [30], which the reader should consult for details. In the phase diagram, it occurs close to the limit where the system becomes homogeneously blue (oxidized), see Figures 4a-c; this is the opposite limit to the retracting wavefront instability. Starting from experimental conditions within the existence balloon ($[H_2SO_4] = 0.3$ M, $[NaBrO_3] = 0.4$ M, [MA] = 0.4 M), we increase a control parameter (the sulfuric acid concentration) so that we gradually approach the homogeneous state.

This instability occurs in the region where one would expect the medium to be oscillatory. At low sulfuric acid concentration ($[H_2SO_4] < 0.6$ M), the spiral is stable, simply rotating. When concentration is increased to $[H_2SO_4] = 0.65$ M, a modulation appears: the distance between successive wavefronts (the local wavelength) varies spatially, instead of being constant. It becomes an oscillating function of the distance to the spiral center, with an amplitude that increases with distance [30]. Far enough from the center, the modulation reaches such a large amplitude that the spiral cannot sustain the deformation and the wave breaks up, nucleating pairs of spiral defects with opposite chirality. This process produces a large number of small spirals around the edge of the stable spiral. Such a process is similar to the one observed in coupled oscillator systems and known as defect-mediated turbulence [58, 59]. It is illustrated in Figure 8, which shows an enlargement of the turbulent region beyond the stable spiral. The wavelength modulation is interpreted as an Eckhaus instability, the most common phase instability of a periodic pattern [60]. The fact that its amplitude increases with distance, without the center being destroyed, is the signature of its convective nature [61, 62].

In general instabilities can be either convective, when small perturbations are carried away faster than they grow, or absolute, when they grow faster than they are carried away. In the latter case, the instability invades the whole space. As our control parameter is increased up to $[H_2SO_4] = 0.8$ M, the stability radius of the spiral decreases. For $[H_2SO_4] > 0.8$ M, the spiral disappears completely into a swarm of spinning spiral defects.

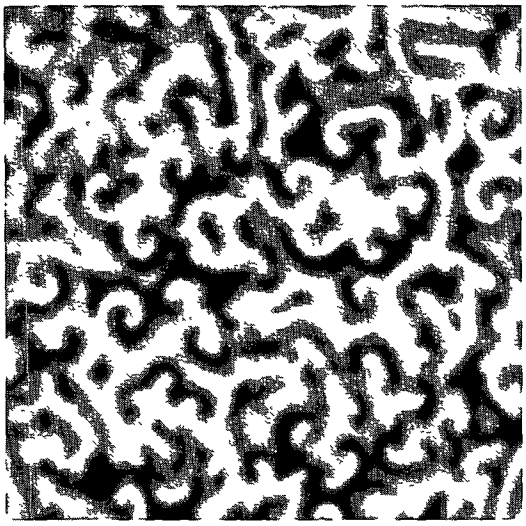

Fig. 8. — An example of the turbulent state beyond the convective instability of the spiral, for $[H_2SO_4] = 0.7$ M, $[NaBrO_3] = 0.4$ M, and [MA] = 0.4 M. The picture is 4.8 mm across.

The boundary of this instability is difficult to define precisely. Nevertheless it systematically occurs when the period of the spiral T_s becomes of the order of 4 s. Hence this transition takes place when T_s decreases down to $T_s = T_{crit}$, where this critical period is in principle a function of the chemical concentrations, though the range of our data is too small to see any variations in T_{crit}. In other words, there is an upper cutoff frequency in the BZ reaction beyond which the medium cannot sustain stable wavetrains. This is in agreement with other investigations of spiral instabilities [63, 64].

This experimentally observed scenario is remarkably well reproduced by the complex Ginzburg Landau equation, which fipermits one to check the theoretical interpretation of the instability mechanisms [65] ([2]). This equation describes the spatio-temporal evolution of the slow varying amplitude of an oscillatory medium close to the onset of oscillation. It has been widely studied, and a similar transition to a spatio-temporal turbulent state is also seen. More details can be found in a recent extensive theoretical study [66].

3.2.3. Transition to Meandering Spirals: Hopf Bifurcation. — The transition to meandering was the first spiral instability recognized and studied as an intrinsic property of the spiral pattern [26]. The term was coined by Jahnke, Skaggs and Winfree to describe the nonpériodic motion of the spiral tip observed in their experiment: instead of following a circular path, the spiral tip ([3]) describes an epicycle-like path [26]. Further experimental [18, 67] and theoretical studies [68–73] have shown that the motion is quasiperiodic, and that the meandering instability is a Hopf bifurcation. It should be noted that all previous studies have mainly focused both on the tip motion and on the instability itself. Few studies have been made on the shape of a meandering spiral, or on the locus of the bifurcation within the spiral phase diagram.

([2]) Rigorously, this comparison is valid close to the onset of the oscillatory state where oscillations are sinusoidal.

([3]) Note that this notion of *spiral tip* requires a precise definition. Experience shows that this is delicate to formulate; it is often considered as the point of maximum curvature.

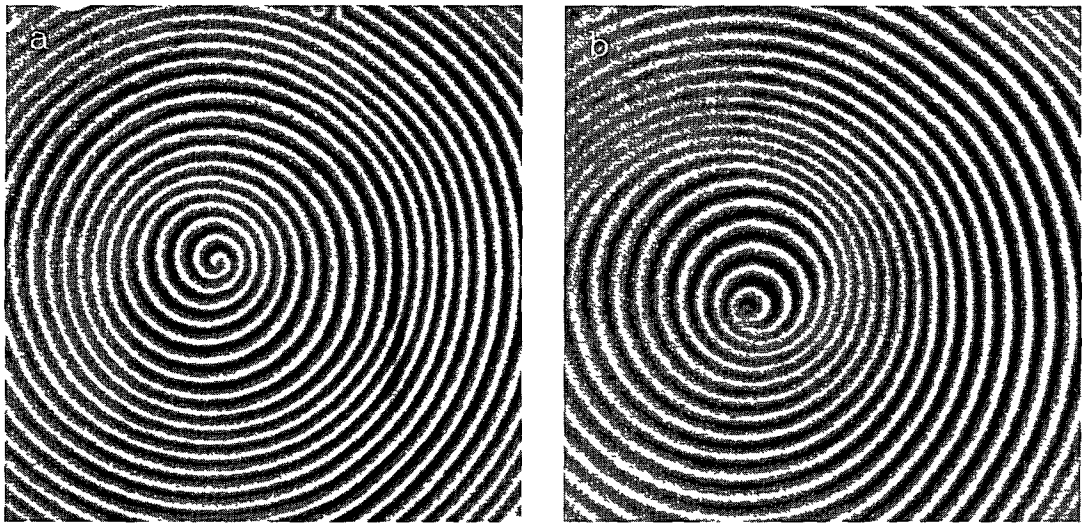

Fig. 9. — Two examples of meandering spirals (see text): (a) retrograde meandering ($[H_2SO_4] = 0.5$ M, $[NaBrO_3] = 0.2$ M, $[MA] = 1.0$ M): (b) prograde meandering ($[H_2SO_4] = 1.0$ M, $[NaBrO_3] = 0.1$ M, $[MA] = 1.0$ M). Compare the chiralities of the spirals and the distortion patterns.

The main characteristics of a meandering spiral appear more clearly in the uneven wavefront spacing, rather than in the detailed analysis of its tip motion. In other words, a single picture of a spiral is enough to recognize whether it is simple or meandering, provided enough turns are present. The history of the quasiperiodic tip motion is somehow inscribed in the shape of the spiral wavefronts.

Although the tip motion not rigorously that of an epicycle, the difference is usually indistinguishable experimentally [18, 67]. Thus the tip executes its primary rotation around a circle (sometimes labeled "moon" [26]) with a frequency f_0, and this circle is itself rotating around a secondary circle ("earth") with a frequency f_1. The ratio f_0/f_1 determines the number of "flower petals" per turn in the spiral tip trajectory. We also define the amplitude of meandering, as the ratio of "earth" circle and "moon" circle r_2/r_1. Two kinds of meandering are possible depending on the relative directions of the two orbiting motions. Either they both orbit in the same direction (*corotating* or *prograde meandering*) or they spin in opposite directions (*contrarotating* or *retrograde meandering*). Although the theory predicts a continuous change from one to the other, experiments have until recently only observed retrograde meandering, which was sometimes referred to as Agladze's rule [74]. We actually observe both kinds, as shown in Figure 9.

At low malonic acid concentration ($[MA] = 0.04$ M), all spirals undergo retrograde meandering. For a fixed bromate concentration, the number of petals and the amplitude are larger at high sulfuric acid concentration than at low. For $[NaBrO_3] = 0.1$ M, the number of petals is 30 for $[H_2SO_4] = 1.0$ M, and 5 for $[H_2SO_4] = 0.1$ M. Plesser *et al.* also report an increase of the number of petals with increasing $[H_2SO_4]$, but observe a decrease in amplitude [67].

At high malonic acid concentration $[MA] = 1.0$ M, the picture is different (see Fig. 4c). First of all, there is a "meandering tongue" within the stable spiral region, where the meandering is either prograde or retrograde, depending on the concentrations. The dynamic behavior of the two types of meandering spirals are similar: their meandering amplitude is small near the

Table II. — *(p_s (μm), T_s (s)) vs. $[H_2SO_4]$ for various $[NaBrO_3]$, at $[MA] = 0.4$ M.*

$[H_2SO_4]$ (M)	$[NaBrO_3]$ (M)									
	0.1		0.15		0.2		0.4		0.6	
	p_s	T_s	p_s	T_s	p_s	T_s	p_s	T_s	p_s	T_s
0.1							1429	92.4	595	25.71
0.2			1511	96.0	1095	58.1	565	17.7	416	11.2
0.3	2200	168.6	925	37.3	721	26.3	423	9.9	345	7.5
0.4	1066	52.6	697	21.9	565	17.4	383	7.3	355	5.8
0.5	888	37.6	589	16.4	481	12.3	331	6.2	323	4.5
0.6	681	23.9	478	11.5	422	9.6	350	5.4	314	3.9
0.7	589	18.9	422	9.53			345	4.6		
0.8	524	15.4	396	7.63	339	6.5				
0.9	464	12.1	385	6.71						
1.0	435	9.8	373	6.06	303	4.5				

onset and increases as the control parameter is changed beyond the onset. The phase diagram obtained for a fixed $[NaBrO_3]$ (see Fig. 4d) is thus similar to the theoretical prediction made in [71]. A more systematic study of the transition between these two types of meandering has since been performed [75].

Note that within the concentration range presented here, we do not observe the "hyper-meandering" seen in computer simulations, where more than two frequencies are needed to describe the tip motion [51]. We have seen some preliminary evidence that, if such meandering exists, it would be at very low malonic acid concentrations.

3.3. Quantitative Results on Simple Spirals. — We now restrict our analysis to simple spirals in the BZ reaction. In this case, pitch and period are well defined quantities, whereas this is not true for meandering spirals.

3.3.1. General Scaling Relations. — For a given point in the appropriate region of parameter space, an initially straight wavefront with a free end will curl up into a simple spiral with a uniquely defined pitch p_s and period T_s. These quantities are determined by the dynamics of the reaction, which depend on the chemical concentrations. What is the selection mechanism? To answer this question, we have measured the pitch and the period of the spiral at each indicated point in Figure 4, using the technique described in Section 2.3. Our measurements allow us to identify the control parameter for the system, and the dependence of the pitch and period on it. To first order, the quantitative laws for spiral selection are scaling relations; the corrections to these relations provide a more detailed dependence on chemical concentrations. Hopefully this framework will eventually be extended to incorporate the case of meandering.

Since in this section we focus uniquely on the data for simple spirals, which are represented by an "S" in Figure 4, the simplest phase plane is Figure 4b, in which no meandering spirals are observed. In this diagram, the pitch ranges from 0.3 mm to 2.5 mm, and the period from 4 s to 200 s; for each point we associate the numbers (p_s, T_s). A compilation of our data can be found in Table II. Though most of our analysis is done for the data in Figure 4b, we also include the simple spirals from Figures 4c-d, which gives an indication of the dependence on [MA].

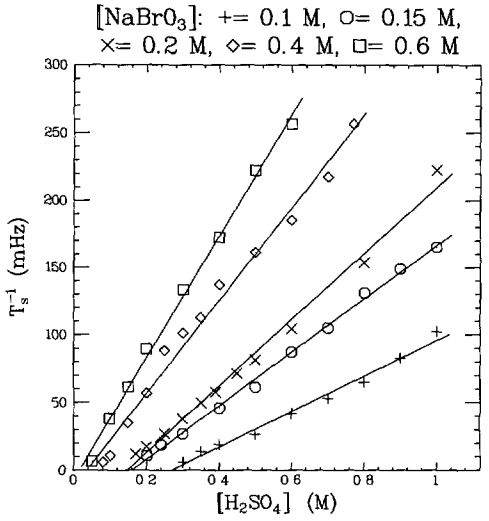

Fig. 10. — The inverse of the spiral period T_s^{-1} *vs.* [H_2SO_4] for several different bromate concentrations at [MA] = 0.4 M (Fig. 4b).

Starting with a simple spiral somewhere in the stable region, its period and pitch diverge as the state of the system approaches the retracting wavefront instability boundary (represented by the black squares in Fig. 4). For concentrations above this line, the inverse of the measured spiral period T_s^{-1} is a linear function of [H_2SO_4], as shown in Figure 10 for each value of [$NaBrO_3$] in Figure 4b. Although the relation is remarkably linear in each case, the slopes and intercepts are different for each bromate concentration. These different lines can be collapsed by plotting T_s^{-1} against the variable

$$\chi \equiv [H_2SO_4] \times [NaBrO_3], \tag{3}$$

as shown in Figure 11. Close to zero, the spiral frequency varies linearly with χ, and vanishes at a finite value of χ, equal within the experimental error to χ_c as defined in equation (2). The spreading at larger values of χ is due to a second order dependence on the chemical concentrations (see Sect. 3.3.2). As a first approximation, the variable χ captures the dependence of the spiral period on the chemical concentrations.

The dependence of T_s on [MA] is found by analyzing the data from Figure 4d. In Figure 12 we plot T_s^{-1} as a function of [H_2SO_4] for all simple spirals in this phase plane. In this case bromate concentration is fixed, so that the rescaling of the x axis to χ would not change the relative positions of the curves. We observe no large displacement of these curves, which would indicate a dependence on [MA], except for a small separation at high [H_2SO_4], which we will discuss in Section 3.3.2. The general fit shows a linear dependence as before. Thus for simple spirals T_s is independent of [MA] to first order, and the general scalings observed in Figures 11 and 12 are summed up by the following experimental law:

$$T_s \sim (\chi - \chi_c)^{-1} \tag{4}$$

We therefore consider χ as the control parameter for the three variable phase space we are studying.

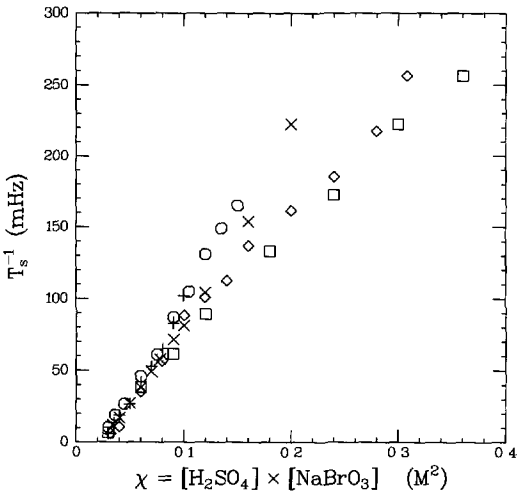

Fig. 11. — The inverse of the spiral period T_s^{-1} *vs.* the rescaled variable $\chi \equiv [NaBrO_3] \times [H_2SO_4]$, for the same data as shown in Figure 10 (also same symbols).

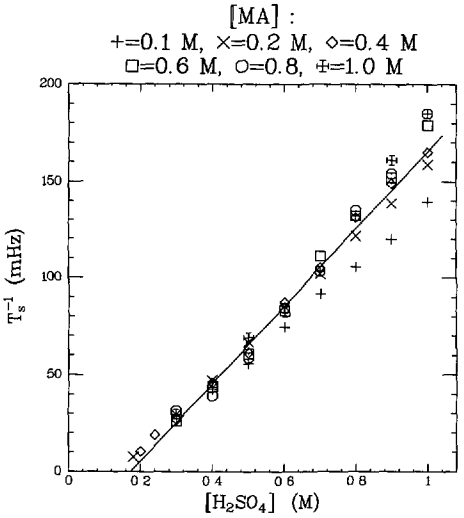

Fig. 12. — The inverse of the spiral period T_s^{-1} *vs.* $[H_2SO_4]$ for several different [MA], at $[NaBrO_3] = 0.15$ M (Fig. 4d).

The selected pitch of the spiral p_s is its most obvious length scale; it is also the wavelength of the emitted waves. Without reference to any chemical concentrations, the dependence of the selected pitch p_s on the period T_s is shown in Figure 13 for the simple spirals we have observed in Figure 4. Remarkably, without any adjustment or normalization, all points follow the same general curve, given by:

$$p_s = (139 \pm 5) \times T_s^{0.51 \pm 0.02}, \tag{5}$$

with p_s in μm and T_s in seconds. From this measurement, we assume the following scaling

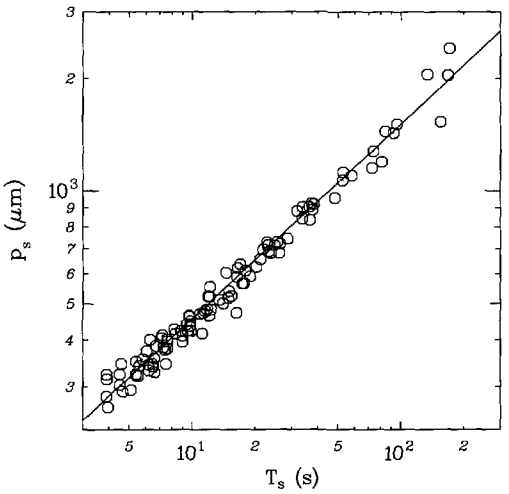

Fig. 13. — The spiral pitch p_s *vs.* the period T_s (log-log plot) for all simple spirals in Figures 4b-d (103 data points). The straight line corresponds to the scaling relation $p \sim T_s^{0.53}$

relation, which we might call the *constitutive relation*:

$$p_s \sim T_s^{1/2} \tag{6}$$

We also conclude from Figure 13 that in the range 0.1 M $<$ [MA] $<$ 1.0 M, the observables of a simple spiral are independent of [MA] to first order, although the concentration of MA does play a role in the transition between simple and meandering spirals, as discussed above.

The scaling relation given by equation (6) is in fact a strong statement on the spiral selection mechanism, since it implies that p_s^2/T_s is a constant. This ratio has the units of a diffusion coefficient, indicating that the spiral is governed essentially by diffusive processes. For all of the simple spirals in the ([H_2SO_4], [MA]) plane of Figure 4d, and for the simple spirals with [$NaBrO_3$] $<$ 0.6 M in Figure 4b, this constant is given by:

$$\frac{p_s^2}{T_s} = 22 \pm 4 \times 10^{-5} \text{cm}^2/\text{s}, \tag{7}$$

For [$NaBrO_3$] $>$ 0.6 M, the value is significantly different and will be discussed in the next section. Since molecular diffusion thus plays a crucial role in the selection mechanism of the spiral, it is natural to consider the dimensionless ratio defined in [51], which we call the *spiral diffusion number*:

$$M_s \equiv \frac{p_s^2}{DT_s}. \tag{8}$$

If we use the value $D \simeq 4.2 \times 10^{-6}$ cm^2/s (see Sect. 2.2), we find $M_s \simeq 52$. Using the accepted value for BZ in solution, $D = 2.0 \times 10^{-5}$ cm^2/s [35], would give $M_s \simeq 10$. The extreme value of $D_\perp = 7 \times 10^{-7}$ cm^2/s measured for a transverse gradient of ions in porous glass [38] gives $M_s \simeq 290$. We will discuss this in Section 4.3. Thus though we cannot report with certainty the value of this selected spiral number M_s with much precision, we emphasize the general result that $p_s \sim T_s^{1/2}$ for all of our spirals, as shown in Figure 13.

For all simple spirals in our experiment, the observables p_s and T_s can be completely specified by the distance in parameter space from the critical line defined by χ_c. There was a hint of

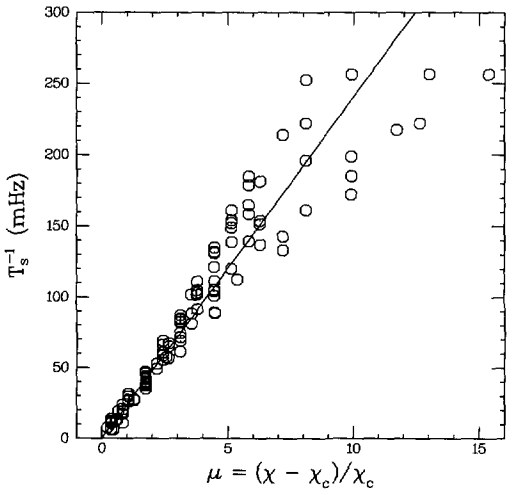

Fig. 14. — The inverse period T_s^{-1} *vs.* μ for all of the simple spirals in our experiment (121 data points).

this possibility in the numerical simulations of [51]. This strong resemblance to the physics of second order phase transitions, with the retracting wavefront instability at the critical point, leads us to define a dimensionless similarity variable μ:

$$\mu \equiv \frac{(\chi - \chi_c)}{\chi_c}, \tag{9}$$

which for our experiments ranges from about 0.2 to 15. In terms of this variable, we show for example the inverse spiral period in Figure 14, for all of the simple spirals we have observed. The linear fit in this figure, and the fit shown in Figure 13 (Eq. (5)) are summarized by the general scaling relations:

$$T_s = T_0 \mu^{-1}; \tag{10}$$

$$p_s = p_0 \mu^{-1/2}, \tag{11}$$

where the time and length scales are given by $T_0 = 41.5 \pm 2.5$ s and $p_0 = 920 \pm 33$ μm. The retracting wavefront instability thus occurs for $\mu \to 0$ and the convective instability for μ large (about 12). We also note from Figure 14 that the scaling is quite accurate for $\mu < 4$, and that for larger values of μ there are systematic corrections, which are discussed in the next section.

3.3.2. Towards a Microscopic Chemical Description of BZ Spirals. — Although the scaling laws in equations (10, 11) provide a concise and simple summary of the characteristics of the selected spiral, they are not exact relations. This is not surprising, since the control parameter χ is symmetric with regard to sulfuric acid and bromate concentrations, whereas it is known that these two species do not play the same chemical role. The asymmetry appears as corrections to the scaling relations: for large enough μ systematic variations are seen, which depend mainly on the bromate concentration. These deviations from a universal scaling law for spirals in the BZ reaction reveal the detailed connection between the macroscopic pattern observables and the underlying chemical mechanisms of the reaction. Although we propose no theoretical framework in which to understand them, these experimental observations provide hints and constraints for a theory of spirals based on the microscopic chemistry of the BZ reaction.

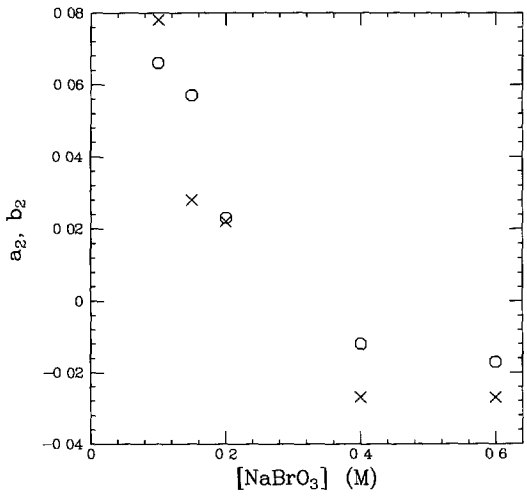

Fig. 15. — The bromate dependent correction coefficients for [MA] = 0.4 M: a_2 (circles), accounting for the correction to the scaling of T_s with μ; b_2 (crosses), accounting for the correction to the scaling of p_s with μ (see the text).

Table III. — *Corrections to scaling. Values of the a_2 and b_2 coefficients, as a function of [NaBrO$_3$], for [MA] = 0.4 M.*

[NaBrO$_3$](M)	0.1	0.15	0.2	0.4	0.6
a_2	0.066	0.057	0.023	−0.012	−0.017
b_2	0.078	0.028	0.022	−0.027	−0.027

Bromate Corrections to Scaling.— We first consider the variations of period as a function of the control parameter μ, at a fixed value of malonic acid concentration. As seen in Figure 11, $T_0/T_s \sim \mu$ for small enough μ, but these curves fan out for large μ, with a systematic dependence on bromate concentration: the lower [NaBrO$_3$], the more concave this curve is. In the absence of any theoretical functional form, and within the precision of our data, the only term we can give is the beginning of a development in powers of μ:

$$T_0/T_s = \mu + a_2\mu^2 + o(\mu^2). \tag{12}$$

where a_2 contains the bromate dependence. In order to obtain the a_2, we make a least mean square fit of T_0/T_s to the functional form given by equation (12), with a_2 being the only free parameter. We check this procedure by making a linear fit to $T_0/T_s - \mu$ as a function of μ^2: the slope in each case is close to the obtained value of a_2, and the intercept with the y-axis is always close to zero.

Results are shown in Figure 15, and listed in Table III. Error bars are difficult to evaluate for numbers that result from so many fits; they are on the order of 20%. Nevertheless, a_2 is clearly a decreasing function of bromate concentration. Though the graph hints at some curvature, we cannot distinguish between a linear or a parabolic dependence, given the imprecision and

the relatively small number of available data points. They are:

$$a_2([NaBrO_3]) = -0.17 \times ([NaBrO_3] - 0.43), \quad (13)$$

$$a_2([NaBrO_3]) = 0.52 \times ([NaBrO_3] - 0.71)([NaBrO_3] - 0.32). \quad (14)$$

where all concentrations are expressed in moles per liter, and the a_2 are dimensionless. The former relation is the simplest, but the latter takes into account the curvature, giving a minimum value for a_2, which might have some chemical meaning. Beyond this, our study is inconclusive, and further measurements are required.

Since the scaling law for the pitch is written $p_0/p_s \sim \mu^{1/2}$, corrections might be written either as powers of $\mu^{1/2}$ or μ. We have found that by considering

$$(p_0/p_s)^2 = \mu + b_2\mu^2 + o(\mu^2), \quad (15)$$

we obtain values of b_2 which are close to the a_2 at each $[NaBrO_3]$ (see Fig. 15). Fitting the data in this way gives:

$$b_2([NaBrO_3]) = -0.19 \times ([NaBrO_3] - 0.36). \quad (16)$$

$$b_2([NaBrO_3]) = 0.72 \times ([NaBrO_3] - 0.70)([NaBrO_3] - 0.26). \quad (17)$$

Note that the near equality $a_2([NaBrO_3]) \simeq b_2([NaBrO_3])$, and the definitions in equations (12) and (15), mean that these bromate corrections cancel in M_s, so that $M_s \simeq p_0^2/DT_0 + o(\mu^2)$. Thus M_s is constant even to second order in μ.

Malonic Corrections to Scaling. — As presented in Section 3.1, the spiral parameters for various malonic acid concentrations, at a fixed bromate concentration, show no [MA] dependence to first order. We have not examined the systematic corrections due to malonic acid which occur within the spread of points in Figure 12.

Corrections to the Constitutive Relation. — Although the scaling relation $p_s \sim T_s^{1/2}$ (Eq. 6) implies a fixed value of the *spiral diffusion constant*

$$D_s \equiv p_s^2/T_s, \quad (18)$$

there are also systematic corrections. They appear as the thick spread of points around the fit in Figure 13, which translate into an 18% variation in the value of p_s^2/T_s (Eq. (7)).

In order to characterize these corrections, we first analyze D_s as a function of χ for fixed [MA]. Since only simple spirals are considered, we focus on the phase diagram for [MA] = 0.4 M (Fig. 4b). For each experimental point, the corresponding value of D_s is plotted as a function of χ in Figure 16. The different curves correspond to different values of $[NaBrO_3]$. To first order, all curves collapse and have the same V-shape, with a minimum at $\chi_{min}([MA] = 0.4\ M) \simeq 0.10\ M^2$. We observe qualitatively that the width of these V-shaped curves increases with $[NaBrO_3]$. Note that we have excluded data for $[NaBrO_3] = 0.6$ M (the highest bromate concentration we have studied) since the behavior is markedly different, as discussed below.

The dependence of χ_{min} with [MA] is obtained by considering the simple spirals in the phase diagram at fixed $[NaBrO_3]$ (Fig. 4d). We find that the curves $D_s(\chi)$ for different values of [MA] have the same V-shape, but the minimum is shifted along the [MA] axis. Subtracting off the value of χ where these minima occur, $\chi_{min}([MA])$, allows the different curves to collapse onto each other, as shown in Figure 17. The variation of χ_{min} appears to be fairly linear with [MA], as shown in Figure 18.

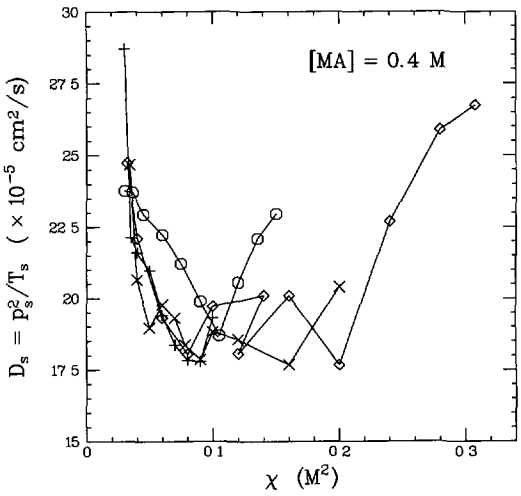

Fig. 16. — The spiral diffusion constant $D_s = p_s^2/T_s$ *vs.* χ for [MA] = 0.4 M. Same symbols as Figure 10.

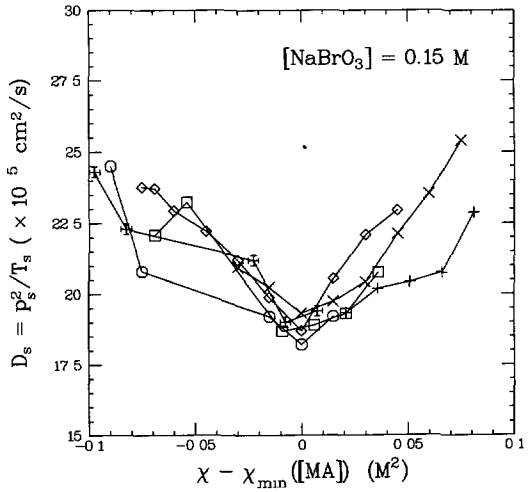

Fig. 17. — The spiral diffusion constant $D_s = p^2/T_s$ *vs.* $\chi - \chi_{min}([MA])$ for [NaBrO$_3$] = 0.15 M. Same symbols as Figure 12.

Thus for the simple spirals in our experiment, the minimum value of D_s is given by

$$D_s(\chi_{min}([MA])) = 18.5 \pm 0.5 \times 10^{-5} \text{ cm}^2/\text{s}, \tag{19}$$

with

$$\chi_{min}([MA]) \simeq 0.082 \times [MA] + 0.065, \tag{20}$$

where all concentrations are expressed in moles per liter. In terms of the dimensionless control

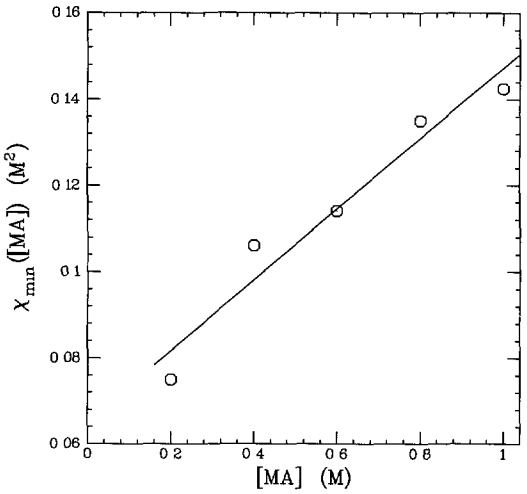

Fig. 18. — The value of the control parameter for which D_s is a minimum, $\chi_{min}([MA])$ *vs.* [MA]. The straight line corresponds to a linear fit (Eq. (20)).

parameter μ, this minimum D_s occurs at (using $\chi_c = 0.022$ M^2):

$$\mu_{min}([MA]) \simeq \frac{[MA]}{0.27} + 2.0, \tag{21}$$

Is there a global cause for this minimum in D_s? Although we have no definite answer to this question, we have made preliminary measurements of the medium itself, which show whether it is excitable or oscillatory. By using the laser to displace the spiral center without allowing it to rotate, we can open a hole where the medium is unperturbed by wave fronts. We then observe whether the medium spontaneously oscillates or not. For [MA] = 0.2 M, we find that the transition occurs around $\chi \simeq 0.08$M^2, in accordance with equation (20). This suggests that $\chi_{min}([MA])$ might correspond to the boundary between an excitable and an oscillatory medium, though no other changes are seen in the spiral characteristics.

A complete description of D_s would require a more thorough study as a function of [$NaBrO_3$]. We have seen quantitatively that [MA] displaces the V curve, whereas [$NaBrO_3$] widens it. But for [$NaBrO_3$] = 0.6 M, the values of p_s^2/T_s are significantly lower than at other concentrations. We have not systematically investigated this effect, but we have two examples from the phase diagrams at [MA] = 0.4 and 1.0 M, shown in Figure 19. Although the minimum value of D_s is significantly lower, the value of χ_{min} where it occurs is still in agreement with the line in Figure 18. For [$NaBrO_3$] = 0.6 M, we find that

$$D_s(\chi_{min}([MA])) = 14.0 \pm 0.5 \times 10^{-5} \text{ cm}^2/\text{s}, \tag{22}$$

using χ_{min} given by equation (20). This difference at higher [$NaBrO_3$] may be the beginnings of another instability, possibly the signature of a boundary of the existence balloon.

3.3.3. Extension to Meandering Spirals. — Both the general scaling relations and the corrections to these relations presented above come from an analysis of simple spirals. How can this framework be extended to the meandering spirals? Here we will only give the beginnings of

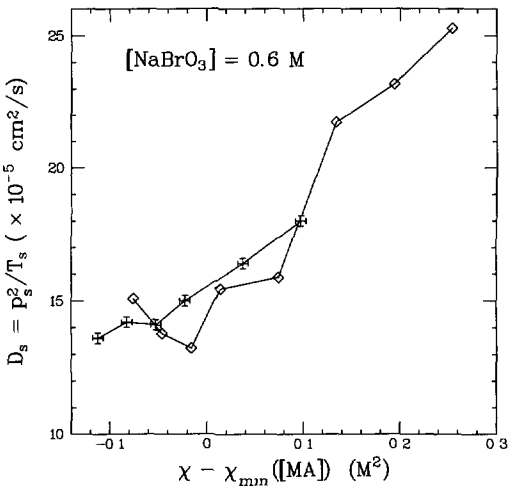

Fig. 19. — The spiral diffusion constant $D_s = p^2/T_s$ *vs.* $\chi - \chi_{min}([MA])$ for $[NaBrO_3] \simeq 0.6$ M.

what might be such an extension. The final result of this endeavor would be a *quantitative* understanding of the different aspects of meandering, including the dependence of the meandering amplitude and frequencies on the chemical concentrations, or control parameters.

The meandering instability is an instability of the spiral core [71, 72], but experimentally this is not straightforward to define. Can we measure some aspect of the spiral core? In order to evaluate its size, we have time averaged images of simple spirals from Figure 4d, for [MA] larger than 0.5 M. For simple spirals between the meandering tongue and the critical line, the averaged image clearly exhibits an unexcited dark region at the center, with a radius of about 10% of the pitch. They are represented by an "O" in Figure 20. We identify this radius with the core radius. For spirals on the other side of the meandering tongue, no dark region was observed ("o" in Fig. 20). This implies that the radius is smaller than one pixel; given the measured values of the pitch, 10% would correspond to a few pixels. We tentatively conclude that the ratio of the core radius to the pitch on this side is smaller than a few percent. This implies a qualitative transition from large-core type near the critical line (μ near 0) to small-core type at larger μ. This agrees with the qualitative picture given by Barkley in his spiral phase diagram [71], and also with the recent definition of "dense" and "sparse" spirals in numerical simulations of spirals in a model for excitable medium [76].

The problem of measurements for meandering spirals is related to the fact that pitch and period now vary with position. As a first attempt, we have measured the minimum and maximum oscillation period (T_{min} and T_{max}) at a single point a few turns from the center of the meandering spiral (so that curvature corrections to the velocity are negligible, see Sect. 4.1). We then include the inverse of these periods in a plot of T_s^{-1} *vs.* $[H_2SO_4]$, as shown in Figure 21. The line is a linear fit to the simple spirals only corresponding to equation (4). From this we find that the *maximum frequency* T_{min}^{-1} (represented by squares) continues to follow the selected spiral period given by equation (10), with the minimum frequency T_{max}^{-1} (asterisks) below. Further quantitative measurements are needed, in particular to characterize the width of this frequency band as χ is varied. However, we do not yet understand *why* a spiral meanders at a given set of concentrations, which is to say we do not understand the role of [MA].

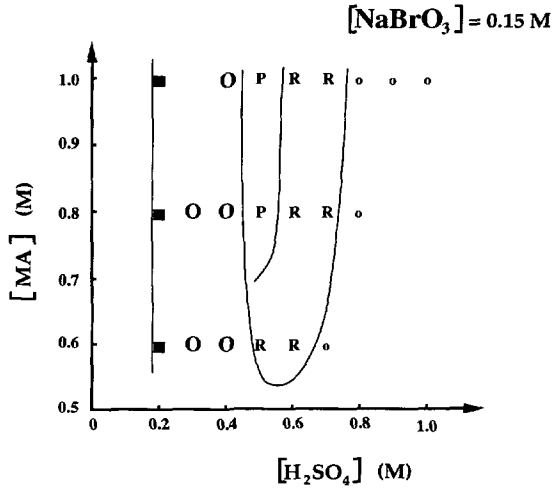

Fig. 20. — Upper part of phase diagram 4d. o: small core simple spiral; O: large core simple spiral; P: prograde meandering spiral; R: retrograde meandering spiral. Other experimental points have not been analyzed.

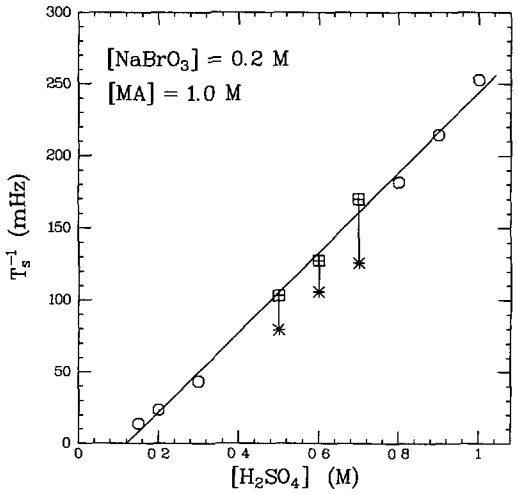

Fig. 21. — The inverse of the spiral period T_s^{-1} ($\odot$) for simple spirals, and the inverse of minimum and maximum periods T_{min}^{-1} ($\boxplus$) and T_{max}^{-1} ($*$) for meandering spirals (see the text), *vs.* $[H_2SO_4]$, at $[NaBrO_3] = 0.2$ M, $[MA] = 1.0$ M.

4. Discussion

4.1. Experimental Comparisons: The Velocity Relation. — To our knowledge, there exist no systematic quantitative studies of spiral waves in an open BZ reactor as a function of the chemical concentrations; the study of meandering by Skinner and Swinney is an exception [18]. However, the dependence of the velocity of a *single* front on these concentrations has been well measured in a number of studies [47, 48, 77–80], allowing for comparison with

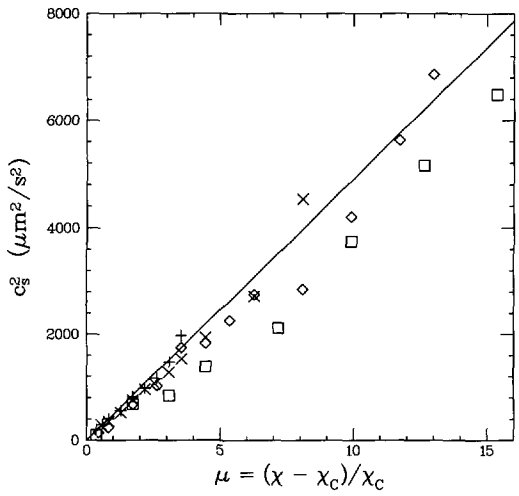

Fig. 22. — The square of the spiral wave velocity $c_s^2 = p_s^2/T_s^2$ *vs.* the dimensionless control parameter μ, for [MA] = 0.4 M. The line corresponds to the scaling relation $c_s^2 = c_0^2\mu$, see equation (23).

our results. From our measurements, we can deduce the velocity of the spiral wavefront using $c_s \equiv p_s/T_s$ [50]. In general, the velocity of a curved wavefront is written as $c = c_p - D\kappa$, where c_p is the velocity of a single plane wave, κ is the curvature of the wavefront, and D is the diffusion constant [54,81,82]. Since $D \simeq 10^{-5}$ cm^2/s, and typically $\kappa \simeq 20$ cm^{-1} for distances beyond one turn from the center, the measured velocity for a spiral ($\simeq 40$ μm s^{-1}) is very close to c_p. Hence we can neglect curvature effects and compare our spiral measurements with the literature values for single plane waves. We should however keep in mind that wavefronts within a spiral are actually interacting, which is represented by the dispersion relation [50].

From equations (10, 11), the spiral wave velocity varies like the square root of the distance to the critical line:

$$c_s = c_0\mu^{1/2}, \tag{23}$$

where $c_0 \equiv p_0/T_0 = 22.2$ μm/s. A plot of c_s^2 *vs.* μ does indeed show a linear relationship as illustrated in Figure 22 for [MA] = 0.4 M; the solid line is equation (23). Note that the points taken at [$NaBrO_3$] = 0.6 M fall systematically below this line, another sign of the possible high bromate transition discussed above. For the other concentrations there is excellent agreement for $\mu < 4$, and small deviations for larger μ.

The experimentally determined scaling relation in equation (23) is similar to the square root law first postulated by Luther in 1906 for the speed of a diffusion limited wave [83], which can be derived from dimensional arguments in the following way. For a reaction Substrate+A+B $\rightarrow$ C with a reaction constant k, one expects the characteristic time scale τ_R to be set by the rate of the reaction: $\tau_R^{-1} = k$[A][B]. Any length in the problem can only come from the diffusion constant of the medium D: the distance diffused in a reaction time is given by $\sqrt{D\tau_R}$. Thus the speed should be $c \sim \sqrt{D\tau_R}/\tau_R \sim \sqrt{Dk}$[A][B].

Such a square root dependence has been found in a number of experiments on single fronts in the BZ reaction, where the wave speed c is usually fit to the function:

$$c = A\chi^{1/2} - c_0, \tag{24}$$

with $\chi \equiv$ [H_2SO_4] $\times$ [$NaBrO_3$], c_0 ranging from 30 to 70 μm s^{-1}, and A from 300 to

500 μm s^{-1} M^{-1} [77, 79, 80, 85]. Analysis of chemical models of front propagation in the BZ reaction [47,48,79,85] as well as more general models [86] justify this functional form, but without the constant c_0. It is merely used as an additional fit parameter, and as far as we know is unjustified, with the exception of a suggestion by Showalter that it is related to the concentration of Br^- [48]. Note that the product χ varies over a small range in most of these studies (the largest being from 0.07 to 0.14 M^2 [77]), and that in addition to equation (23), a linear relation $c \sim \chi$ is often also a good fit of the data.

In our experiments, the velocity c_s is consistent with a square root dependence on $\chi - \chi_c$, with χ varying from 0.02 to 0.36 M^2. The value of χ on the "critical line", χ_c, plays the role of the constant c_0 in equation (24), defining the concentrations for which $c = 0$. Thus the speed of waves within the spiral have the same scaling as the single wavefront speed, indicating an internal self-similarity of spirals over a wide concentration range; this was also suggested by a recent measurement of the dispersion relation $c(T)$ in a BZ open reactor [50].

4.2. Models for Spiral Behavior. — There are several different theoretical approaches to the dynamics of spirals in reaction-diffusion systems, and in particular to the problem of spiral selection. To compare with our experimental measurements, we focus on the models which may be suited to spirals in the BZ reaction. In the first two sections we consider two different approaches: chemical modeling and singular perturbation methods. In both cases we evaluate the predictions in light of our experimental results, though it is not our intention to give a comprehensive review. In the third section, we discuss possible reasons for the differences between these models and our observations.

Note that we do not describe two other approaches which have proven successful in different areas of spiral dynamics, but which cannot be quantitatively compared to our results. The first one is a kinematic theory developed by the Russian school [54, 87, 88]. The other one is the normal form approach of Barkley [71, 72], which successfully provided a framework for the understanding of the meandering instability; it included a spiral phase diagram qualitatively similar to those in Figures 4c-d. In particular, the large-core spirals are next to the existence boundary, and close to the prograde meandering spirals (as in Fig. 20), which is also the organization observed in the Oregonator model [51].

4.2.1. Chemical: The FKN Model and the Oregonator. — A coherent, simplified model of the chemical mechanisms underlying the BZ reaction was proposed by Field, Kőrös, and Noyes in 1972, and is known as the FKN model [89–91]. Kinetic equations can then be derived from this model, and a simplified version is given by three coupled differential equations known as the Oregonator [47, 92]. It was derived for well-stirred batch reactions where there are no concentration gradients; in these cases it is in excellent quantitative agreement with experiment [90]. It has also been applied to spatially extended systems by the inclusion of diffusion terms; this is generally believed to be sufficient, though no theoretical reflection seems to have been made on this point. Nevertheless, this chemical reaction-diffusion model indicates the possible relevant concentrations to spiral dynamics. In this section we compare our experimental results with numerical simulations of spirals using the Oregonator. This indicates some fundamental disagreements between the measurements and these chemically-based models.

Originally the FKN model was derived for the oxidation of malonic acid catalyzed by cerium. It can also be adapted to other variants of the reaction, but the rate constants of the elementary reactions have to be reconsidered. The approximations which lead to the Oregonator may then need to be modified, resulting in different models [79, 93–95]; unfortunately, these distinctions are often not specified in the literature. The Oregonator also explicitly assumes that a number of species concentrations, including malonic acid, are constant. Although this

allows in principle for the steady state regimes that are obtained in an open reactor, some care should be taken with any quantitative comparison between the Oregonator and experimental results from an open system. There is notably no flow rate or other mechanism in the Oregonator which maintains the nonequilibrium conditions, whereas such things are obviously present experimentally. This difference may in fact be crucial [96]. However, in what follows we consider only our experimental conditions, namely the oxidation of malonic acid in the presence of ferroin. A rigorous justification of the spiral simulations with which we compare our results would require a careful re-examination of the models, which we will not attempt here.

Amidst the many elementary reactions that take place in the BZ reaction, the FKN model distinguishes three processes: bromide consumption (A), the autocatalytic stage (B), and regeneration (C). Each process is controlled by the concentration level of a particular species, with a particular role in the oscillation cycle. Process A involves the transformation of the bromide ion (Br^-) into different oxidized forms. Since this ion is an *inhibitor* for the autocatalytic process B, the role of process A is essentially Br^- removal. When $[Br^-]$ reaches a lower critical value, process B starts, leading to a rapid increase in the amount of $HBrO_2$, which is called the *activator*. An additional result of this reaction is the oxidization of the catalyst, which transforms ([4]) Fe^{2+} into Fe^{3+} Process C transforms the catalyst back into its reduced state (Fe^{2+}), at the expense of oxidizing the malonic acid. But this latter reaction produces Br^- ions, which block process B and restart process A; the cycle is complete. In the overall reaction, the malonic acid is degraded, which is related to the decrease of the free energy as required by thermodynamics.

The heart of this mechanism is the autocatalytic process B, which controls the leading front of a single wave moving into a fully recovered medium [47,48]. Its overall stoichiometry is:

$$BrO_3^- + HBrO_2 + 2Fe^{2+} + 3H^+ \rightarrow 2HBrO_2 + 2Fe^{3+} + H_2O. \tag{25}$$

An analysis of the intermediate steps show that its effective time constant is given by [91]:

$$\tau_R^{-1} = k[H^+][BrO_3^-], \tag{26}$$

where k varies between 10^2 $M^{-2}s^{-1}$ [86] and 10^4 $M^{-2}s^{-1}$ [47,48]. This effective rate sets the time scale for the wave, and one expects the speed of a front to be given by $c \sim \sqrt{D/\tau_R}$ (Luther's law, see Sect. 4.1), which is nearly equation (24). This indicates the fundamental role played by the product $[H^+][BrO_3^-]$, which is essentially our χ (Eq. (3)).

Based on the FKN model, a set of coupled differential equations can be written for the three intermediate products that characterize each process [47,94]. These equations are known as the Oregonator:

$$\epsilon_1 \frac{dx}{d\tau} = x - x^2 - y(x-q), \tag{27}$$

$$\epsilon_2 \frac{dy}{d\tau} = -qy - xy + fz, \tag{28}$$

$$\frac{dz}{d\tau} = x - z, \tag{29}$$

where $x \sim [HBrO_2]$, $y \sim [Br^-]$, and $z \sim [Fe^{3+}]$. The concentration variables, the time τ and the parameters ϵ_1, ϵ_2, and q are all normalized by average chemical concentrations and rate constants [24]. The f which appears in equation (28) is not directly related to the

([4]) For simplicity, we represent the state of the entire catalyst (ferroin or ferriin) by that of the metal ion.

Table IV. — *Tyson's "Lo" constant rates for the Oregonator (from [94]).*

k_J	k_2	k_3	k_4	k_5
$1\ M^{-1}s^{-1}$	$10^6\ M^{-2}s^{-1}$	$2\ M^{-3}s^{-1}$	$2\times10^3\ M^{-3}s^{-1}$	$10\ M^{-2}s^{-1}$

concentrations, and represents a partial knowledge of the actual chemistry involved in process C. It is thus taken as a free parameter, which from chemical arguments is between 0 and 4 [51]. The three dimensionless parameters are given by [26,94]:

$$\epsilon_1 = \frac{k_J}{k_5}\frac{[\text{organics}]}{[H^+][BrO_3^-]}, \tag{30}$$

$$\epsilon_2 = \frac{2k_Jk_4}{k_2k_5}\frac{[\text{organics}]}{[H^+]^2[BrO_3^-]}, \tag{31}$$

$$q = \frac{2k_3k_4}{k_2k_5}. \tag{32}$$

where [organics] = [BrMA] + [MA], and the k_i are the various rate constants defined in [94]. Following [51], we consider the version with Tyson's "Lo" parameters, see Table IV.

These parameters are typically: $\epsilon_1 \sim 4\times10^{-2}$, $\epsilon_2 \sim 2\times10^{-4}$, and $q \sim 8\times10^{-4}$ [94]. Since $\epsilon_2 \ll \epsilon_1$, time scales are well separated and the y variable can be considered at its equilibrium value $y = fz/(q+x)$. Thus equations (27–29) become the two-variable Oregonator:

$$\epsilon_1\frac{dx}{d\tau} = x - x^2 - fz\frac{x-q}{x+q}, \tag{33}$$

$$\frac{dz}{d\tau} = x - z, \tag{34}$$

with the parameters ϵ_1 and q still as defined in equation (30) and (32). Since q depends only on the nature of the chemical reaction, it is fixed. But ϵ_1 and f can vary, and are usually considered as two independent parameters [26,51], with $\epsilon_1 \ll 1$ and $f \sim 1$. They are both determined by the chemical concentrations of the reagents, though the exact dependence is not known.

The qualitatively important features of the two variable Oregonator are best seen in its nullclines, represented in Figure 23. The nullcline $dx/d\tau = 0$ has an h-shape, whereas that for $dz/d\tau = 0$ is linear. We only consider the case where they have a single intersection, which is the fixed point. The relative position of the nullclines, which depends on the parameter f, determines whether the point is unstable (the medium is oscillatory) or stable (the medium is excitable). The relative speed of evolution on the branches of the cycle is set by ϵ_1; it is the ratio of the typical time scales of the "slow" reaction to the "fast" one. Many studies have been devoted to this model (see [22]).

In order to allow for the study of spatial patterns in extended systems, the diffusive terms $D_x\nabla^2x$ and $D_z\nabla^2z$ are added to equations (33) and (34). With this modification, the Oregonator has been successful in qualitatively reproducing the same spiral behavior observed in experiments. The most complete survey to date of simple and meandering spirals in this model was carried out by Jahnke and Winfree [51]. For fixed values of $q = 0.002$, $D_x = 1.0$, $D_z = 0.6$ (based on the molecular weights of $HBrO_2$ and ferroin), they surveyed spiral dynamics, including p_s and T_s, in the two dimensional parameter space (ϵ_1, f). Since their simulation did not include enough spiral turns to measure p_s directly, it was obtained by combining the measured

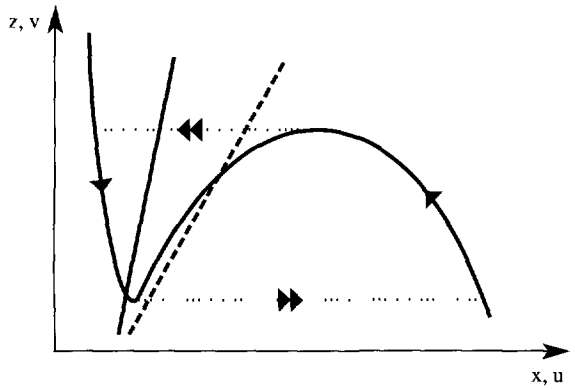

Fig. 23. — The shape of the nullclines for the two variable Oregonator (Eqs. (33–34)). The solid straight line correspond to the excitable case ($f \simeq 4$); the dashed one to the oscillatory case ($f \simeq 1$). The dotted line visualizes the relaxation oscillations. The arrows represent the relative speed. This is also the shape of the nullclines for equations (37–38).

T_s with the dispersion relation from a 1-D circular simulation. Also, the measurements for both simple and meandering spirals were treated together.

From a general qualitative point of view, there are common features between their phase diagram and quantitative relations and ours. Indeed, they observe a boundary for the existence of spirals, where both pitch and period (λ_0 and τ_0 in their notation) diverge as power laws. They also observe well defined regions of different dynamical behavior, notably, simple and meandering spirals. In addition, the relevant parameter, though not explicitly written, is said to be the distance from the divergence boundary.

This boundary constitutes a well defined feature for matching to our results. In the parameter region studied by Jahnke and Winfree, it occurs at high values of f, corresponding to an excitable fixed point in a chemically reduced state. Our critical line is close precisely to the homogeneous reduced state (see Figs. 4a-c). Moreover, our preliminary measurements of the spiral core (see Fig. 20) show that close to the retracting wavefront instability, the spirals are of the large-core type, which seems to be what Jahnke and Winfree observe based on our estimates from [51]. A finer comparison between theories and experiments would require the knowledge of the ratio of the core radius to the spiral pitch in the Oregonator, but this has apparently not been measured.

A closer look at their results, however, reveals a number of qualitative inconsistencies that rule out a full agreement. First, the phase diagram of such a model (Fig. 9 of [51]) is essentially two-dimensional, whereas ours has a conspicuous three-dimensional structure; at the best, the Oregonator's phase diagram is a projection of ours. In their phase diagram, most conditions lead to meandering spirals, whereas experimentally we see the opposite. This suggests that ϵ_1 and f are not likely to give the right scaling. In addition, they have not tried to scale their results with the distance to the boundary (a function of ϵ_1 and f), instead focusing on the limit as ϵ_1 goes to zero; this limit corresponds to that of a sharp wavefront.

Finally we note that the scalings with ϵ_1 reported by Jahnke and Winfree,

$$T_s \sim \epsilon_1^{1/3}, \tag{35}$$

$$p_s \sim \epsilon_1^{1/6}, \tag{36}$$

also lead to the constitutive relation, equation (6). However, the spiral diffusion number

$M_s = p_s^2/DT_s$ (Q in their notation), which they also measured directly, varies from 72 to 900. We discuss this further in Section 4.3.

The spatially extended Oregonator thus shows both similarities and disagreements with our experimental results, and also with previous theories; Jahnke and Winfree write in their conclusion: "we have not been able to interpret our results quantitatively in terms of theory" [51]. Nevertheless, the Oregonator is well known to give satisfactory quantitative agreement with well-mixed experiments (no spatial dimensions). This may mean that simply adding diffusion terms to the original Oregonator misses some aspects of spatially extended patterns. Interpretation of our experiment may also require a more detailed analysis of the experimental conditions: though our spiral patterns are embedded in the thin porous glass, there are also strong perpendicular concentration gradients since the chemicals are not fed symmetrically into the two chambers of the cell. We discuss this in Section 4.2.3

4.2.2. Asymptotics: Singular Perturbations Methods. — Although spirals are experimentally easy to produce in the BZ reaction, mathematically they pose a difficult problem. Two main questions have attracted attention: given a set of reaction-diffusion equations, is it possible to prove that a simply rotating spiral solution exists? If it does exists, what is the selection mechanism? Much theoretical work has been devoted to these questions [82, 97].

A particularly fruitful approach comes from what is known as the singular perturbation limit. This approach reformulates the spiral selection problem for two coupled equations into a free-boundary problem, in the limit of a small parameter which is the ratio of reaction time scales ϵ.

Although once again it is difficult to connect experimental results to these analyses, comparison can still be made with some of their consequences. We begin by briefly describing the basis of the approach. Consider a generic representation of two coupled reaction-diffusion equations:

$$\frac{\partial u}{\partial t} = \frac{f(u,v)}{\tau_u} + D_u \nabla^2 u, \tag{37}$$

$$\frac{\partial v}{\partial t} = \frac{g(u,v)}{\tau_v} + D_v \nabla^2 v, \tag{38}$$

where u and v are the time and space dependent chemical concentrations, τ_u and τ_v are characteristic reaction times for the u and v variables, respectively, and the functions $f(u,v)$ and $g(u,v)$ describe the reactions. Usually $f(u,v)$ and $g(u,v)$ have nullclines similar to those illustrated in Figure 23: note that the Oregonator model given by equations (33–34) is a particular case of these equations. For the diffusion constants we use the notation $\delta \equiv D_v/D_u$, and $D \equiv D_u$. The small parameter is defined as the ratio of the time scales: $\epsilon \equiv \tau_u/\tau_v$. The equations are then nondimensionalized by the time and length scales τ_v and $\tau_v\sqrt{D/\tau_u}$ respectively, leading to:

$$\frac{\partial u}{\partial t} = \frac{1}{\epsilon} f(u,v) + \epsilon \nabla^2 u, \tag{39}$$

$$\frac{\partial v}{\partial t} = g(u,v) + \delta\epsilon \nabla^2 v, \tag{40}$$

where now t and ∇ are non dimensional coordinates. These equations are the starting point for most theoretical studies, and for Fife's conjecture on the selected spiral solution. The singular perturbation theory considers the case where ϵ goes to zero; this implies a vanishingly small reaction zone, which follows the dynamics of the slow variable.

Geometrical. — Starting from the general two equation system 39-40, where one variable reacts much faster than the other, Keener and Tyson have formulated a geometric model for spirals in reaction-diffusion systems [82, 98]. They provide a selection mechanism by requiring that the spiral solution should satisfy both the dispersion relation and another "critical" relation, arising from the constraint imposed by curvature on the velocity.

They assume that both variables are diffusing with the same diffusion coefficient, thus $\delta = 1$. Since most of their results do not give an explicit analytic form, and since numerical integration is necessary to obtain final results, they use the two variable Oregonator model (Eqs. (33-34)) to compare with the experimental results of Winfree [99] and Müller *et al.* [100].

The dispersion relation is first calculated in a one-dimensional model. Because of the structure of the nullclines, at the lowest order in ϵ, the fast variable u jumps between two possible values, whereas v has a slower dynamics. A traveling wave, or pulse, is made of three broad parts separated by narrow regions where the u gradients are large. In the broad regions, u is close either to its quiescent or to its excited value. The dispersion relation links the pulse velocity to its duration (or period), which is approximated by the time spent in the slow dynamics part. The velocity is obtained by constraining the leading wavefront to remain at a fixed distance from the wave back. It is expressed in terms of integrals of implicit functions, and has to be calculated for specific models. The detailed case of the Oregonator is treated in [101].

The critical relation relates the normal velocity c_N to the local curvature κ, through diffusion. It is written as:

$$c_N = c(v_0) - \epsilon\kappa, \tag{41}$$

where $c(v_0)$ is a velocity that only depends on the value of the v variable along the spiral, v_0. Otherwise this equation is similar to the "eikonal" equation, whereby the velocity of a curved front is equal to that of a plane front plus a term proportional to the curvature. If the simple assumption of negligible curvature is made, then equation (41) becomes c_N =constant. The solution is then the involute of a circle, which is known to agree well with experimentally observed spirals far enough from their center [15, 39, 49, 102]. To account for curvature effects close to the center, a differential equation relating the variations of the local wavenumber with the polar angle to the normal velocity and the local curvature has to be written. A similar, though somewhat simpler, approach was used in 1951 to describe the spiral around a screw dislocation in crystal growth [103].

To solve the resulting equation, boundary conditions must be given. What happens at the center near the spiral tip is a difficult problem, whereas the solution around a hole is simpler. Keener and Tyson employ a convenient way to approximate the full problem. They assume a fictitious inner boundary at a radius r_0 from the center, which plays the role of a hole boundary for the outer part, and solve the tip problem inside this disk. They find a critical relation that is written in physical units (see Eq. 5.8 of [98]):

$$\frac{r_0^2}{DT_s} = \frac{1}{\alpha_* M_s}(m_* - \frac{2\pi}{M_s}), \tag{42}$$

where $M_s = p_s^2/DT_s$, with p_s the pitch and T_s the period of the selected spiral, D the diffusion coefficient, and the two numerically determined constants $m_* \simeq 0.330958$ and $\alpha_* \simeq 0.097$.

For the case when r_0 is very small, this equation becomes to lowest order $M_s = 2\pi/m_* \equiv M_* \simeq 18.99$. Keener and Tyson wrote that this result "is intriguing because it is independent of the chemical composition of the excitable reagent" [98]. This agrees well with our observation that M_s is approximately constant for all simple spirals, although the value we find is larger: $M_s \simeq 52$. In their 1988 paper, Tyson and Keener warn that, if

the radius is large enough, equation (42) might not be valid any more [82]. Implications are discussed in Section 4.3, along with the interpretation of the observed variations in M_s in terms of a finite-sized core radius r_0.

Fife Scaling. — These singular perturbation methods received a strong impetus when Fife showed that there might be a unique scaling solution to the system (Eqs. (39-40)) if the space and time variables (x, t) are further rescaled as

$$x' = \frac{x}{\epsilon^{2/3}}, \quad t' = \frac{t}{\epsilon^{1/3}}. \tag{43}$$

Then ϵ scales out from the resulting equation; this is known as the Fife scaling [97, 104, 105]. It has now been checked in a number of particular cases of various δ [52, 106–112], that from here a simply rotating spiral solution may be obtained, whose overall scale is set by ϵ.

Note that the Fife scaling predicts the same constitutive relation as we have found experimentally (Eq. (6)). Thus the spiral diffusion number M_s is a constant:

$$M_s = \frac{p_s^2}{DT_s} = \frac{1}{D}\frac{(\tau_v\sqrt{D/\tau_u})^2}{\tau_v}\frac{p^2}{T} = \frac{p'^2}{T'} = \text{constant}. \tag{44}$$

In other words, the ϵ dependence cancels for the particular scaling choice given by equation (43), a property of the Fife scaling which to our knowledge has not been previously noted. We will discuss this further in Section 4.3.

However, most theoretical studies are concerned with the scaling of the solution in the Fife scaling limit ($\epsilon \to 0$). This corresponds to spirals with small pitch (short wavelength), fast rotation period (high frequency), and slow wavefront speed [82]. In particular, it implies that the dependence of the spiral rotation period T_s is given by

$$T_s \sim \tau_v \epsilon^{1/3} \tag{45}$$

Our results give a different picture: the spiral parameters depend on the distance in parameter space to the retracting wavefront instability, given by $\mu = (\chi - \chi_c)/\chi_c$. The limit $\mu \to 0$, where we observe scaling, is the limit of large pitch, slow rotation period (low frequency), and slow speed. We conclude that, as far as the BZ reaction is concerned, the Fife scaling limit seems to be the inappropriate. In fact, experimentally the fast spiral limit is in a sense interrupted by the convective instability to defect-mediated turbulence. Thus the parameter dependence of the spiral dynamics are organized in a very different way than the Fife scaling approach. It may be that such solutions do occur in some system, or in the BZ reaction in another limit, but at least in our experiments we see no crossover to a new scaling before the convective instability. We are led to conclude, unfortunately, that the mathematically convenient limit is not the physically meaningful one.

Though most of these studies focus on the scaling with ϵ, while the other quantities in the model remain fixed, there is another relevant parameter: the so-called dimensionless excitability Δ [52, 112]. This quantity characterizes the phase space structure of the system; it is proportional to the range of variation of the slow variable v within one pulse. At low excitability it is also proportional to the velocity of the planar wave front. Karma [52] has shown that there exists a single control parameter $B = (g/\alpha^2)\epsilon/\Delta^3$ for spiral solutions, where g and α are model dependent constants of order unity. If one assumes that the wavefronts do not interact within a spiral, a number of analytical results can be derived for the single diffusive case ($\delta = 0$) [52, 112]. In particular, spirals should exist at low B, with a transition to retracting fingers occurring for $B > B_c$, where the rotation period diverges.

This description bears some resemblance to our results. Since the fronts we observe are well defined, it is likely that a proper description of our experimental spirals requires $\epsilon \ll 1$. Using Karma's approach, our results could then be qualitatively interpreted as corresponding to spirals in the model with a constant ϵ and a varying Δ. However, there remain a number of quantitative differences between his predictions and our observations; in particular his approach does not produce the observed scaling laws for T and p.

4.2.3. Possible Origins of Disagreement with 2-D Models. — We have seen in the previous sections that theories and models provide to some extent a qualitative account of the spirals we have observed, but that quantitative comparison fails. We suggest two sources of this failure: inadequacies internal to the theories themselves, and differences between the models and the actual experimental system.

Theoretical Difficulties. — We first discuss the general two variable systems describing generic excitable media. As we have seen, whether the slow field is diffusing or not, the Fife scaling leads to a unique spiral solution, and provides a positive answer to the problem of selection. However a number of difficulties remain with this solution [107, 109, 111]. When compared to direct numerical simulations of the model, it appears that some variables, like the frequency, behave essentially as expected, whereas others, like the core size, show a significant departure from predictions.

The stability of the Fife solution is also an unsolved problem, since it is known that the core is unstable to a single real mode [111]. It has been suggested that this instability could be related to the meandering instability that has been observed in simulations at small ϵ [57, 69, 73]. But the meandering instability arises through a Hopf bifurcation [70], *i.e.* with a complex conjugate pair of unstable modes. These two results are in contradiction.

Finally, as experimentalists we also wonder whether one of the most basic assumptions of the Fife solution is relevant: that successive wavefronts do not interact.

Modeling the Experimental System. — Our results also lead us to speculate on the source of differences with the microscopic chemical models. As briefly mentioned earlier, the FKN model and the Oregonator have not been derived for open reactors: terms describing the input and output flows are missing in the equations, which could play a role in the stability properties of the system. In addition, it might well be that our concentrations have exceeded the ranges for which these models have been developed.

However, a more important difference may lie in the description of the reactor itself. Modeling of real open reactors used in reaction-diffusion experiments (specifically for Turing patterns) is only recent [96, 113]; experimental observations had first been qualitatively explained in terms of the ideal two-dimensional theories. But the growing accuracy of the experiments has lead to the conclusion that quantitative agreement can only be obtained with a more accurate modeling of the apparatus. This means taking into account the geometry of the experimental cell, with the finite thickness and the chemical gradients of the reaction medium.

This approach might also be appropriate for our spirals. The observed pattern is actually an integration over the porous glass thickness; the transverse information on the wave structure is lost. Nonetheless there are strong concentration gradients in that direction. It may be that there are different concentration layers within the disk thickness, which if separated would be in different dynamical regimes; in the experiment, they are diffusively coupled. A similar situation gives rise to the crescent-shaped waves in the chemical pinwheel experiments [34, 114], and other experimental effects of transverse gradients have also been observed [115, 116]. The resulting global behavior, and its bifurcation structure, would then require more advanced models than the standard two-dimensional models. Taking into account the third dimension

opens the way for a large number of possible new phenomena —transverse size of the reacting zone, wave structure and dynamics, with possible instabilities through a "third dimensional" escape [117]— that need further experimental and theoretical studies.

4.3. Quantitative Analysis of the Spiral Diffusion Number M_s. — Given that quantitative studies of spirals are rare, and that most experiments have been conducted with different chemical concentrations, it is no surprise that mainly qualitative comparisons have been made. In order to compare spirals with different characteristics, one needs dimensionless similarity variables which describe the spiral in terms of the relevant physical properties of the medium. Of course, the difficulty lies in finding what is relevant. Given that pitch and period are the two most characteristic quantities of the spiral, and that diffusive processes play a major role in the spatial aspects of the system, the variable $M_s \equiv p_s^2/DT_s$, our *spiral diffusion number* (Eq. (8)), is a reasonable first choice. This was realized by Winfree, who has tabulated values of M_s (which he calls Q) for both experimental work and simulations [26, 51, 57]. The quantity was in fact first introduced in models of spiral formation in crystal growth [103]. It might also be used to compare spirals in any system where diffusion plays a role, for instance in liquid crystals [118, 119], or the phase patterns in Rayleigh-Bénard convection [97, 120].

Previous experimental measurements, performed only in closed systems, have found M_s ranging from 20 to 180 [19.55, 57]. This may in fact be related to the aging of the system: in one experiment it was shown that M_s increases with time as the solution ages and the spiral slows down [55]. Simulations of the Oregonator also show that M_s can have values ranging from 70 to 900 [51]. The inconclusiveness of previous measurements of M_s may be the reason why more studies have not been undertaken.

As remarked previously, the constitutive relation $p_s \sim T_s^{1/2}$ (Eq. (6)) translates into a constant value of M_s. The corrections to the scaling (see Sect. 3.3.2) imply variations in M_s, which can be plotted as a contour map in the phase diagrams of Figure 4. An example is shown in Figure 24 for the ([H_2SO_4], [MA]) plane (at fixed [$NaBrO_3$] = 0.15 M). The dashed line corresponds to the minima of M_s described by equation (20). There is also a change in the core size, and possibly also a change in the medium from oscillatory to excitable (Sect. 3.3.2), but further experimental study is needed to clearly connect these diverse observations. It also remains for a theoretical analysis of the spatially extended BZ reaction to provide the explanation for these topographical features of parameter space.

A possible interpretation for the variations in M_s is found in the critical relation from the Keener-Tyson model (Eq. (42)). We first rewrite it for the normalized core radius $R \equiv r_0/p_s$:

$$R(M_s) = \frac{R_0}{M_s}\sqrt{1 - \frac{M_*}{M_s}}, \tag{46}$$

where $M_* = 2\pi/m_* \simeq 18.99$ is the predicted minimum M_s corresponding to $r_0 = 0$, and $R_0 \equiv (2\pi/(\alpha_* M_*))^{1/2} \simeq 1.847$. If the radius is large enough, equation (46) is not valid and should be replaced by another relation [82]. In the limit of diffusionless medium, this new relation (see Eq. (25) of [82]) can be transformed to give M_s as a function of the normalized core radius:

$$M_s(R) = \frac{1}{2}\frac{\pi R(5 - 8\pi R) + \sqrt{\pi R(4 - 7\pi R)}}{R(1 - 2\pi R)^2}, \tag{47}$$

which must then be inverted to get $R(M_s)$. The two resulting functions $R(M_s)$ given by equations (46) and (47) are plotted in Figure 25. In both cases, there is a minimum value for M_s of about 20.

Equation (46) (curve (a) in Fig. 25) gives a maximum value for the core radius of about 3% of the selected pitch p_s at $M_s \simeq 25$, which then decreases down to about 1% for larger M_s; this

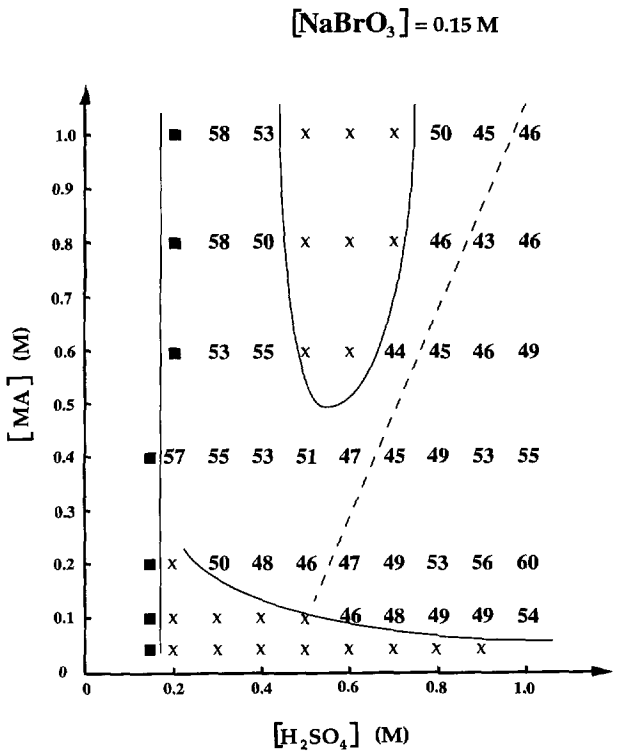

Fig. 24. — The spiral diffusion number $M_s = p_s^2/DT_s$ in the ($[H_2SO_4]$, [MA]) plane, for fixed $[NaBrO_3] = 0.15$ M. The X's correspond to meandering spirals, and the dashed line to the location of $\chi_{min}([MA])$.

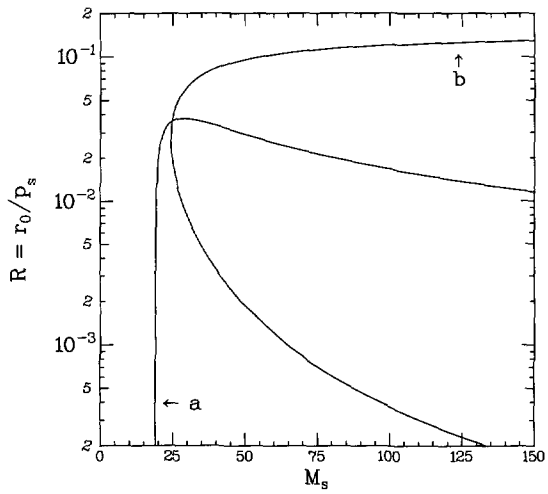

Fig. 25. — Reduced core radius R *vs.* spiral diffusion number M_s. Note the logarithmic scale in y; (a), plot of equation (46); (b), plot calculated from equation (47).

gives an overall variation in r_0 of a factor 3. On the other hand, the curve $R(M_s)$, as obtained from equation (47) implies large variations in R. For a given M_s, two values are possible: either R is of the order of 10% or a few percent. Without any reason to choose one of these curves over the other, curve (b) seems in better agreement with the observations of the core size change and the V-shaped variation of M_s.

In Figure 24, we see that M_s does not have a monotonic variation, but that its minimum roughly follows the edge of the meandering tongue. This is compatible with equation (47) if one allows for a shift in M_s. Suppose that the "knee" is at $M_s \simeq 50$; then the observed variation of M_s could correspond to a monotonic variation in R. The large core radii would occur on the upper branch, and the small ones on the lower one. In addition, since the observed constitutive relation does not show large variations in M_s, whereas the core radius varies over at least one order of magnitude, such a dependence is consistent with the vertical tangent in $R(M_s)$ at the minimum value of M_s.

As noted above, the Fife scaling implies a constant value of M_s, but it does not specify what this value is. A value was obtained by Karma in a study of the FitzHugh-Nagumo equations, a commonly used model of excitable medium, for the specific case $\delta = 0$ in equations (39-40) [107]. It is identical to the one found by Keener and Tyson [98]: $M_s = 18.99$. This should be compared to our measured value $M_s \simeq 52$. A comparison should also be possible with the numerical results of Winfree for the FitzHugh-Nagumo model [57]. He finds variations in M_s between 21 and 144, without any clear minimum, although the size of the core changes in a way qualitatively similar to what we observe. Though some caution should be taken since his values also incorporate meandering spirals, there are many possible reasons for the difference between these values. The bottom line is probably that the phenomenon is not understood.

4.4. Comparison with Closed Reactors. — As we have noted throughout this article, most previous experiments on the BZ reaction have been conducted in closed reactors, making it difficult to directly compare our data with previously published ones. These experiments often seem to give meandering spirals, whereas large portions of our explored phase diagram contain simple spirals. This might be due to the consumption of malonic acid. We have indeed observed that at low malonic acid, all spirals are meandering (see Figs. 4a and 4d). This agrees qualitatively with the observed evolution: in a closed reactor, an aging spiral always evolves from simple to larger and larger meandering [55,121]. Further investigation of the role of [MA] in open reactors should lead to a better understanding of spirals in closed reactors.

4.5. Speculations on Spirals in Reaction-Diffusion Systems. — Given that the agreement between our data and any one of the current proposed models for spirals in reaction-diffusion systems is at best partial, one might well wonder what sort of a model *would* agree with our data. In fact the scaling relations we have observed amounts to a connection between the microscopic level (chemical concentrations, represented by χ or μ) and the macroscopic level (spiral observables, p_s and T_s). By following a line of reasoning based on our scaling relations, we are led towards the general form of the reaction-diffusion model which would describe our data, though not to the model itself. The speculations presented here clarify the implications of our observations, and in particular highlight the analogy to second order phase transitions.

We begin with the general reaction-diffusion equations given in equations (37–38). For simplicity we will demonstrate our arguments using only one equation:

$$\frac{\partial u}{\partial t} = \frac{f(u,v)}{\tau} + D\nabla^2 u, \tag{48}$$

where τ is a typical chemical timescale, and D the diffusion constant as before. As we are interested in the selected spiral solution to this equation, we non-dimensionalize the variables by the time and space scales p_s and T_s, respectively. This leads to:

$$\frac{1}{T_s}\frac{\partial u}{\partial t'} = \frac{f(u,v)}{\tau} + \frac{1}{p_s^2} D\nabla'^2 u, \tag{49}$$

which can be rewritten, dropping the primes,

$$\frac{\partial u}{\partial t} = \frac{T_s}{\tau} f(u,v) + \frac{DT_s}{p_s^2}\nabla^2 u \tag{50}$$

$$= \frac{T_s}{\tau} f(u,v) + \frac{1}{M_s}\nabla^2 u. \tag{51}$$

The spiral diffusion number M_s appears explicitly as the multiplier of the diffusion term, in much the same way as the Reynolds number in the Navier-Stokes equations for fluid flow (see *e.g.* [122]). Thus the constitutive relation $p_s \sim T_s^{1/2}$ which implies a constant M_s, also implies that the diffusive term is the same relative size for all concentrations. In other words, $M_s = \text{const}$ implies a self-similarity which here appears as the independence of equation (51) of any chemical concentration.

Note that the non-dimensionalization leading to equation (51) can be written explicitly in terms of μ using equations (10–11):

$$x' = \frac{x}{p_s} \sim \mu^{1/2} x, \quad t' = \frac{t}{T_s} \sim \mu t. \tag{52}$$

A comparison of this with equation (43) shows clearly that the Fife scaling is in the opposite limit as the natural one implied by the observations, which leads to the parameter μ.

It is interesting to consider this argument further, given our measured scaling $T_s \sim \mu^{-1}$ Since M_s is independent of μ (to first order), as is the left hand side of equation (51), the prefactor of $f(u,v)$ must be as well. Thus $\tau \sim \mu^{-1}$ Our original equation in lab frame coordinates becomes:

$$\frac{\partial u}{\partial t} = \mu f(u,v) + D\nabla^2 u. \tag{53}$$

We recover a simple Landau equation, which clarifies the link to second-order phase transitions.

The consideration of the second variable v of course adds a complication to this derivation, since one would then have to choose which time scale is related to T_s. In addition, the argument which results in equation (53) does not treat the wave propagation boundary as distinct from the spiral boundary (see [56,57]). However this is only the beginnings of a model which might describe our experimental results, and should only be taken as giving the flavor of a future critical scaling theory for spiral patterns.

5. Conclusion

As a result of our study, is it now possible to prepare a spiral with an arbitrary set of characteristics? In other words, can we specify beforehand what chemical concentrations should be mixed in order to obtain a spiral with a given pitch and period? Well, our answer is a partial "yes".

As far as spatial open reactors are concerned, an unexpected simple picture of spirals in the Belousov-Zhabotinsky reaction has emerged. The selected spiral is a sort of critical pattern,

which can to first approximation be described by two scaling relations: one linking the period with the chemical species, and the other linking the pitch with the period. In this sense, the pitch and period cannot be independently chosen. The spiral existence domain is delimited on one side by a critical line, which also defines the onset of the retracting wavefront instability, and at the other end by a lower bound on the rotation period, below which the spiral becomes unstable to defect mediated turbulence. This means that we have experimentally found the relevant parameters. Our measurement of the corrections to these scaling relations open the way both for a finer link with models for the chemical reactions and for a possible physical interpretation in terms of the core size.

Although meandering spirals must somehow fit into this picture, subtler considerations apparently need to be taken into account to predict where in the chemical phase diagram the meandering instability takes place. This remains an open question.

We have seen that a large part of our framework comes from observation only. Neither chemical models nor geometrical theories provide a full quantitative understanding of our measurements. Current analytical approaches, which seem satisfactory when restricted to a qualitative comparison with experiments, fail to give a full coherent description. The discrepancy might be rather deep since our data show that most analytical work actually considers the opposite limit to the one where we observe our scaling laws! In other words, our observations have lead us to define a parameter μ which ranges from 0 to 16. Our attempts to connect this μ to the "small parameter" of various models indicate that the two are not compatible.

Partial failure of the chemical modeling is probably due to the lack of quantitative data on spirals. Although our experiments supply material to confront further studies, we are still far from an exhaustive knowledge. First, we have only explored a part of parameter space, since we only varied three concentrations. Of the parameters which remain, the influence of the catalyst concentration, the flow rate, and the diffusion constant of the medium (which would include the temperature), should definitely be studied. But even within the survey presented here, several open questions remain. It is certainly necessary to explore the phase diagram at low malonic acid concentration; this could clarify the relation between open and closed systems. Also, we have not systematically tracked the transition from an oscillatory to an excitable medium, since no difference is seen in the spiral; this might give informative insight to the underlying chemistry.

Nonetheless, our data indicate that general principles of spiral dynamics should be sought. We have found that the spiral is a kind of critical, self-similar structure within the chemical parameter space, so it is likely that it obeys some simple extremization rule, such as the maximization of malonic acid consumption. In the end, a realistic model of the experimental setup may be needed to clarify the arrangement of chemical concentrations within the reactor.

Given the efficiency of the normal form analysis, which successfully predicts a full phase diagram from a localized study, it would be interesting to couple the known five ODEs which describe the motion of the tip [71] with a continuous two dimensional phase field describing the rest of the spiral. This approach would only add one PDE, which would be simpler than the original starting point of two coupled PDEs.

Although these results seem to raise more new questions than answer old ones, our hope is that they will stimulate further study, theoretical as well as experimental.

Acknowledgments

We would like to thank D. Barkley, P. Coullet, V. Croquette, J.-M. Gilli, G. Goren, V. Hakim, G. Huyet, V. Krinsky, J. Lega, S. Maurel, A. Pumir, S. Rica and V. Voignier for help and discussions, and especially A. Bernoff, V. Gáspár, A. Karma, and J. Lega for comments on the

manuscript. We thank the referees for constructive comments. A.B. acknowledges the support of N.S.F. Grant No. INT-9406090, and of a Chateaubriand Fellowship.

References

[1] Thompson D'A.W., On Growth and Form (Cambridge University Press, Cambridge, England, 1942).
[2] Höfer T. and Maini P.K., *Nature* **380** (1996) 678.
[3] Kondo S. and Asai R., *Nature* **376** (1995) 765.
[4] Murray J.D., Mathematical Biology (Springer-Verlag, Berlin, second edition, 1993).
[5] Glansdorff P. and Prigogine I., Structure, Stabilité et Fluctuation (Masson, Paris, 1971).
[6] Nicolis G. and Prigogine I., Self-Organization in Non-Equilibrium Systems (Wiley, New-York, 1977).
[7] Turing A.M., *Phil. Trans. R. Soc. London B* **237** (1952) 37.
[8] Koch A.J. and Meinhardt H., *Rev. Mod. Phys.* **66** (1994) 1481.
[9] Feynman R.P., Leighton R.B. and Sands M., The Feynman Lectures on Physics, volume II, chapter 41 (Addison-Wesley, Reading, 1964).
[10] Meron E., *Phys. Rep.* **218** (1992) 1.
[11] Davidenko J.M., Kent P. and Jalife J., *Physica D* **49** (1991) 182.
[12] Self-organization: autowaves and structures far from equilibrium, V.I. Krinsky, Ed. (Springer-Verlag, Berlin, 1984).
[13] Winfree A.T., When Time Breaks Down (Princeton University Press, 1987).
[14] Zaikin A. and Zhabotinsky A., *Nature* **225** (1970) 535.
[15] Winfree A.T., *Science* **175** (1972) 634.
[16] Chemical waves and patterns, R. Kapral and K. Showalter, Eds. (Kluwer Academic Publishers, Dordrecht, 1995).
[17] Kshirsagar G., Noszticzius Z., McCormick W.D. and Swinney H.L., *Physica D* **49** (1991) 5.
[18] Skinner G.S. and Swinney H.L., *Physica D* **48** (1991) 1.
[19] Tam W.Y., Horsthemke W., Noszticzius Z. and Swinney H.L., *J. Chem. Phys.* **88** (1988) 3395.
[20] Belousov B.P., A periodic reaction and its mechanism, in "Sbornik Referatov po Radiatsionni Meditsine" (Medgiz, Moscow, 1958) p. 145., English translation in [23], pp. 605–613.
[21] Winfree A.T., *J. Chem. Educ.* **61** (1984) 661.
[22] Scott S.K., Chemical Chaos (Clarendon Press, Oxford, 1991).
[23] Oscillations and Traveling Waves in Chemical Systems, R.J. Field and M. Burger, Eds. (Wiley, New York, 1985).
[24] Field R.J., Experimental and mechanistic characterisation of bromate-ion-driven chemical oscillations and traveling waves in closed systems, in "Oscillations and Traveling Waves in Chemical Systems", R.J. Field and M. Burger, Eds. (Wiley, New York, 1985) pp. 55–92.
[25] Noszticzius Z., McCormick W.D. and Swinney H.L., *J. Phys. Chem.* **91** (1987) 5129.
[26] Jahnke W., Skaggs W.E. and Winfree A.T., *J. Phys. Chem.* **93** (1989) 740.
[27] Yamaguchi T., Kuhnert L., Nagy-Ungvárai Zs., Müller S. C. and Hess B., *J. Phys. Chem.* **95** (1991) 5831.

[28] Hodgkin A.L. and Huxley A.F., *J. Physiol.* **117** (1952) 500.
[29] Krinsky V.I., *Pharmac. Ther. B* **3** (1978) 539.
[30] Ouyang Q. and Flesselles J.-M., *Nature* **379** (1996) 143.
[31] Ouyang Q. and Swinney H., *Chaos* **1** (1991) 411.
[32] Castets P., Dulos E., Boissonade J. and De Kepper P., *Phys. Rev. Lett.* **64** (1990) 2953.
[33] Ouyang Q., Boissonade J., Roux J.C. and De Kepper P., *Phys. Lett. A* **134** (1989) 282.
[34] Noszticzius Z., Horsthemke W., McCormick W.D., Swinney H.L. and Tam W.Y., *Nature* **329** (1987) 619.
[35] Foerster P., Müller S.C. and Hess B., *Proc. Natl. Acad. Sci. USA* **86** (1989) 6831.
[36] Voignier V., Private communication.
[37] Amemiya T., Nakaiwa M., Ohmori T. and Yamaguchi T., *Physica D* **84** (1995) 103.
[38] Ouyang Qi, Li R., Li G. and Swinney H.L., *J. Chem. Phys.* **102** (1995) 2551.
[39] Belmonte A. and Flesselles J.-M., *Europhys. Lett.* **32** (1995) 2.
[40] Lázár A., Noszticzius Z., Försterling H. and Nagy-Ungvárai Z., *Physica D* **84** (1995) 112.
[41] Balzani V. and Carassiti V., Photochemistry of coordination compounds (Academic Press, London, 1970) p. 165.
[42] Gáspár V., Bazsa G. and Beck M., *Z. phys. Chemie* **264** (1983) 43.
[43] Belmonte A. and Flesselles J.-M., *Phys. Rev. Lett.* **77** (1996) 1174.
[44] Braune M. and Engel H., *Chem. Phys. Lett.* **204** (1993) 257.
[45] Kuhnert L., *Naturwissenschaften* **73** (1986) 96.
[46] Steinbock O. and Müller S.C., *Phys. Rev. E* **47** (1993) 1506.
[47] Field R.J. and Noyes R.M., *J. Amer. Chem. Soc.* **96** (1974) 2001.
[48] Showalter K., *J. Phys. Chem.* **85** (1981) 440.
[49] Müller S.C., Plesser T. and Hess B., *Physica D* **24** (1987) 87.
[50] Belmonte A., Flesselles J.-M. and Ouyang Q., *Europhys. Lett.* **35** (1996) 665.
[51] Jahnke W. and Winfree A.T., *Int. J. Bifurcation and Chaos* **1** (1991) 445.
[52] Karma A., Velocity selection in two-dimensional excitable media: from spiral waves to retracting fingers. In "Growth and Form, Nonlinear Aspects", M. Ben Amar, P. Pelce and P. Tabeling, Eds. (Plenum Press, New York, 1991) pp. 271–283.
[53] Karma A., *Phys. Rev. Lett.* **66** (1991) 2274.
[54] Mikhailov A.S., Davydov V.A. and Zykov V.S., *Physica D* **70** (1994) 1.
[55] Nagy-Ungvárai Zs. and Müller S.C., *Int. J. Bifurcation and Chaos* **4** (1994) 1257.
[56] Barkley D. and Kevrekidis I.G., *Chaos* **4** (1994) 453.
[57] Winfree A.T., *Chaos* **1** 1991 303.
[58] Coullet P., Gil L. and Lega J., *Phys. Rev. Lett.* **62** (1989) 1619.
[59] Coullet P. and Lega J., *Europhys. Lett.* **7** (1988) 511.
[60] Eckhaus W., Studies in Nonlinear Stability (Springer-Verlag, New-York, 1965).
[61] Aranson I.S., Aranson L., Kramer L. and Weber A., *Phys. Rev. A* **46** (1995) R2992.
[62] Huerre P. and Monkewitz P.A., *Ann. Rev. Fluid Mech.* **22** (1990) 473.
[63] Bär M., Hildebrand M., Eiswirth M., Falcke M., Engel H. and Neufeld M., *Chaos* **4** (1994) 499.
[64] Voignier V., Experimental observation of convective instability in chemical excitable system, *in preparation* (1996).
[65] Kramer L., Hynne F., Graae Sørenson P. and Walgraef D., *Chaos* **4** (1994) 443.
[66] Chaté H. and Manneville P., *Physica A* **224** (1996) 348.
[67] Plesser T., Müller S.C. and Hess B., *J. Phys. Chem.* **94** (1990) 7501.
[68] Barkley D., Kness M. and Tuckerman L.S., *Phys. Rev. A* **42** (1990) 2489.
[69] Barkley D., *Physica D* **49** (1991) 61.
[70] Barkley D., *Phys. Rev. Lett.* **68** (1992) 2090.

[71] Barkley D., *Phys. Rev. Lett.* **72** (1994) 164.
[72] Barkley D., Spiral meandering, in "Chemical waves and patterns", R. Kapral and K. Showalter, Eds. (Kluwer Academic Publishers, Dordrecht, 1995) pp. 163–190.
[73] Karma A., *Phys. Rev. Lett.* **65** (1990) 2824.
[74] Agladze K.I., Panfilov A.V. and Rudenko A.N., *Physica D* **29** (1988) 409.
[75] Li G., Ouyang Qi, Petrov V. and Swinney H.L., *Phys. Rev. Lett.* **77** (1996) 2105.
[76] Krinsky V., Hamm E. and Voigner V., *Phys. Rev. Lett.* **76** (1996) 3854.
[77] Dajka J., Károly T., Nagy I.P., Gáspár V. and Noszticzius Z., *J. Chem. Soc. Faraday Trans.* **92** (1996) 2897.
[78] Kuhnert L. and Krug H.-J., *J. Phys. Chem.* **91** (1987) 730.
[79] Nagy-Ungvárai Zs., Tyson J.J. and Hess B., *J. Phys. Chem.* **93** (1989) 707.
[80] Wood P.M. and Ross J., *J. Chem. Phys.* **82** (1985) 1924.
[81] Kessler D.A. and Levine H., *Europhys. Lett.* **12** (1990) 465.
[82] Tyson J.J. and Keener J.P., *Physica D* **32** (1988) 327.
[83] Luther R., *Z. Elektrochemie* **12** (1906) 596. English translation [84].
[84] Luther R., *J. Chem. Educ.* **64** (1985) 740.
[85] Eager M.D., Santos M., Dolnik M., Zhabotinsky A.M., Kustin K. and Epstein I.R., *J. Phys. Chem.* **98** (1994) 10750.
[86] Tyson J.J. and Manoranjan V.S., The speed of propagation of oxidizing and reducing wave fronts in the Belousov-Zhabotinskii reaction, in "Non-Equilibrium Dynamics in Chemical Systems", C. Vidal and A. Pacault, Eds. (Springer-Verlag, Berlin, 1984.) pp. 89–93.
[87] Mikhailov A.S., Foundations of Synergetics I (Springer-Verlag, Berlin, second edition, 1990).
[88] Zykov V.S., Simulation of Wave Processes in Excitable Media (Manchester University Press, New York, 1987).
[89] Field R. J., Kőrös E. and Noyes R.M., *J. Am. Chem. Soc.* **94** (1972) 8649.
[90] Gray P. and Scott S.K., Chemical Oscillations and Instabilities (Clarendon Press, Oxford, 1994).
[91] Scott S.K., Oscillations, Waves and Chaos in Chemical Kinetics (Oxford University Press, Oxford, 1994).
[92] Field R.J. and Noyes R.M., *J. Chem. Phys.* **60** (1974) 1877.
[93] Showalter K., Noyes R.M. and Bar-Eli K., *J. Chem. Phys.* **69** (1978) 2514.
[94] Tyson J.J., A quantitative account of oscillations, bistability and traveling waves in the Belousov-Zhabotinskii reaction, in "Oscillations and Traveling Waves in Chemical Systems", R.J. Field and M. Burger, Eds. (Wiley, New York, 1985) pp. 93–145.
[95] Zhabotinsky A.M., Buchholtz F., Kiyatkin A.B. and Epstein I.R., *J. Phys. Chem.* **97** (1993) 7578.
[96] Dufiet V. and Boissonade J., *Phys. Rev. E* **53** (1996) 4883.
[97] Cross M.C. and Hohenberg P.C., *Rev. Mod. Phys.* **65** (1993) 851.
[98] Keener J.P. and Tyson J.J., *Physica D* **21** (1986) 307.
[99] Winfree A.T., Unpublished results, Can be found in [98, 101].
[100] Müller S.C., Plesser T. and Hess B., *Science* **230** (1985) 661.
[101] Dockery J.D., Keener J.P. and Tyson J.J., *Physica D* **30** (1988) 177.
[102] Lázár A., Noszticzius Z., Farkas H. and Försterling H.-D., *Chaos* **5** (1995) 443.
[103] Burton W.K., Cabrera N. and Frank F.C., *Phil. Trans. Roy. Soc. Lond. A* **243** (1951) 299 .

[104] Fife P.C., Propagator-controller systems and chemical patterns, in "Non-Equilibrium Dynamics in Chemical Systems", C. Vidal and A. Pacault, Eds. (Springer-Verlag, Berlin, 1984) pp. 76–88.
[105] Fife P.C., *J. Stat. Phys.* **39** (1985) 687.
[106] Bernoff A.J., *Physica D* **53** (1991) 125.
[107] Karma A., *Phys. Rev. Lett.* **68** (1992) 397.
[108] Keener J.P., *Physica D* **70** (1994) 61.
[109] Kessler D.A. and Kupferman R., *Physica D* **97** (1995) 509.
[110] Kessler D.A., Levine H. and Reynolds W.N., *Phys. Rev. Lett.* **68** (1992) 401.
[111] Kessler D.A., Levine H. and Reynolds W.N., *Physica D* **70** (1994) 115.
[112] Pier B., Spirales dans les milieux excitables, Master's thesis, École Normale Supérieure de Lyon (Lyon, France, 1995). Unpublished, in French.
[113] Barillot E., Structures de Turing dans les systèmes chlorite-iodure-acide malonique et dioxyde de chlore-iode-acide malonique: Études théoriques et modélisation numérique, PhD thesis (Université Bordeaux I, France, 1996). Unpublished.
[114] Dulos E., Boissonade J. and De Kepper P., *Physica A* **188** (1992) 120.
[115] Zhabotinsky A.M., Müller S. and Hess B., *Physica D* **49** (1991) 47.
[116] Zhabotinsky A.M., Györgyi L., Dolnik M. and Epstein I.R., *J. Phys. Chem.* **98** (1994) 7981.
[117] Voignier V., Dynamique et contrôle de vortex en milieux excitables, PhD thesis (Université de Nice Sophia-Antipolis, France, 1997). Unpublished.
[118] Gilli J.-M., Morabito M. and Frisch T., *J. Phys. II France* **4** (1994) 319.
[119] Vierheilig A., Chevallard C. and Gilli J.-M., *Phys. Rev. E* **55** (1997) 7128.
[120] Bodenschatz E., de Bruyn J., Ahlers G. and Cannell D., *Phys. Rev. Lett.* **67** (1991).
[121] Krüger F., Nagy-Ungvárai Zs. and Müller S., *Physica D* **84** (1995) 95–102.
[122] Tritton D.J., Physical Fluid Dynamics (Clarendon Press, Oxford, second edition, 1988).